

Optimizing laser processing for the production of advanced materials

Luke Bond

Main supervisors: Magnus Engholm

Co-supervisors: Henrik Andersson, Nicklas Blomquist

Department of Engineering, Mathematics and Science Education

Thesis for Licentiate degree in Engineering Physics

Mid Sweden University

Sundsvall, 2024-11-27

Akademisk avhandling som med tillstånd av Mittuniversitetet i Sundsvall framläggs till offentlig granskning för avläggande av teknologie licentiatexamen onsdagen den 15 januari, 10:00, i sal O102, Mittuniversitetet Sundsvall. Seminariet kommer att hållas på engelska.

Optimizing laser processing for the production of advanced materials

© Luke Bond, 2024-11-27

Printed by Mid Sweden University, Sundsvall

ISSN: 1652-8948

ISBN: 978-91-89786-89-9

Department of Engineering, Mathematics and Science Education
Mid Sweden University, Holmgatan 10, 851 70, Sundsvall
Phone: +46 (0)10 142 80 00

Mid Sweden University Licentiate Thesis 207

Acknowledgements

Completing this licentiate thesis has been a remarkable journey, and I am deeply grateful to everyone who has supported me along the way.

I extend my heartfelt thanks to my main supervisor, Magnus Engholm, for his exceptional guidance, expertise in laser material processing, and mentorship, which have been invaluable to my growth as a researcher. I am also grateful to my co-supervisors, Henrik Andersson and Nicklas Blomquist, for their steady encouragement and insightful contributions. Special thanks to Jonas Örtegren for his project leadership and direction and to Magnus Hummelgård for his invaluable knowledge of material characterization, batteries, and graphene, which broadened my understanding.

I sincerely thank Manisha Phadatare for introducing me to battery testing methods and Ghadir Razaz and Shahrzad Rastabi for sharing their expertise in electrochemical research. To my friends and fellow PhD students, Ali Hamad and Mehdi Saatlu especially, thank you for your support and the many discussions that made this journey easier.

To my parents and family, your unwavering love and encouragement have been the foundation of my achievements. Finally, to my life partner, Tokio Melin, your love, patience and belief in me have been my anchor and source of strength.

This work would not have been possible without all of you, and I am profoundly grateful.

Dedicated to my partner, friends, and family – this work is a testament to your love, encouragement, and endless support. I couldn't have done it without you.

Table of contents

Abstract	vi
Summary in Swedish	vii
List of papers	viii
List of acronyms	ix
1 Introduction	1
1.1 Problem statement.....	2
1.2 Research objective	2
1.3 Scope	3
1.4 Thesis outline	3
1.5 Papers included in this thesis	4
2 Laser material processing	7
2.1 Introduction to laser material processing	7
2.2 Types of laser systems	12
2.3 Laser applications in material processing.....	13
2.4 Challenges and opportunities.....	13
2.5 Related work	14
3 Experimental	17
3.1 Laser setups.....	17
3.2 Characterization methods	18
4 Selective laser sintering of polymer-graphene composites	19
4.1 Selective laser sintering	19
4.2 Conductive polymers and selective laser sintering.....	20

4.3 Fabrication of conductive polymers via selective laser sintering	21
4.4 Laser parameter selection and optimization	22
5 Laser processing of graphite-based anodes	27
5.1 Lithium-ion batteries.....	27
5.2 Graphite anodes.....	27
5.3 Electrode material refinement	29
5.4 Optimization of laser parameters.....	30
6 Synthesis of rare earth-doped nanoparticles via laser.....	35
6.1 Pulsed laser ablation in liquid	35
6.2 Selection of target material for pulsed laser ablation in liquid .	37
6.3 Choice of laser system.....	37
6.4 Synthesis of Yb:YVO ₄ nanoparticles	38
7 Conclusion and future work.....	43
7.1 Conclusion.....	43
7.2 Social and ethical considerations	44
7.3 Future work.....	45
7.4 Author's contributions.....	48
Bibliography	49

Abstract

Lasers, with their unparalleled precision and control, have become vital tools across numerous industries, offering transformative potential for the development of advanced materials. In this research, laser-assisted techniques were employed to develop and optimize functional materials for industrial and energy applications. By leveraging the unique properties of laser light, significant advancements were achieved in three key areas. First, selective laser sintering was employed to create electrically conductive polymer-graphene composites, demonstrating promising electrical conductivity, crucial for applications requiring electromagnetic compatibility. Second, rare-earth-doped nanocrystals were synthesized using ultrashort laser pulses, achieving precise control over nanoparticle size and morphology while maintaining consistent stoichiometry with the bulk material. This synthesis offers potential for applications in photonics due to the stability and tailored properties of the nanocrystal. Third, laser-assisted processing was applied to modify nanographite and nanographite-silicon composite anode materials for lithium-ion batteries. The laser-induced nanoporous structure in graphite-based anodes led to significant improvements in fast charging capabilities and specific capacity. Additionally, the optimization of silicon distribution within the nanographite matrix enhanced battery performance and cycling stability. These findings illustrate the versatility and efficacy of laser-assisted processing in tailoring material properties to meet the growing demands of advanced applications, offering a pathway to the development of next-generation materials with enhanced functionalities.

Summary in Swedish

Lasrar, med sin oöverträffade precision och kontroll, har blivit viktiga verktyg inom många industrier, och erbjuder transformativ potential för utveckling av avancerade material. I denna forskning användes laserstödda tekniker för att utveckla och optimera funktionella material för industriella och energitillämpningar. Genom att utnyttja laserljusets unika egenskaper uppnåddes betydande framsteg inom tre nyckelområden. Först användes selektiv lasersintring för att skapa elektriskt ledande polymer-grafenkompositer, som visar lovande elektrisk ledningsförmåga, avgörande för tillämpningar som kräver elektromagnetisk kompatibilitet. För det andra syntetiserades sällsynta jordartsmetall-dopade nanokristaller med hjälp av ultrakorta laserpulser, vilket uppnådde exakt kontroll över nanopartikelstorlek och morfologi samtidigt som konsekvent stökiometri bibehölls med bulkmaterial. Denna syntes erbjuder potential för tillämpningar inom fotonik på grund av nanokristallens stabilitet och skräddarsydda egenskaper. För det tredje användes laserassisterad bearbetning för att modifiera nanografitt och nanografitt-kiselkompositanodmaterial för litiumjonbatterier. Den laserinducerade nanoporösa strukturen i grafitbaserade anoder ledde till betydande förbättringar av snabbbladningskapacitet och specifik kapacitet. Dessutom förbättrade optimeringen av kiselfördelningen i nanografittmatrisen batteriets prestanda och cykelstabilitet. Dessa resultat illustrerar mångsidigheten och effektiviteten hos laserassisterad bearbetning för att skräddarsy materialegenskaper för att möta de växande kraven från avancerade applikationer, vilket erbjuder en väg till utvecklingen av nästa generations material med förbättrade funktionaliteter.

List of papers

This thesis is based on the following papers, as attached in Part B:

Paper I: Electrically conductive polymer-graphene composite material for selective laser sintering additive manufacturing

Luke Bond, Henrik Andersson, Jonas Örtegren, Magnus Larsson and Magnus Engholm

L. Bond, H. Andersson, J. Örtegren, M. Larsson, and M. Engholm, "Electrically conductive polymer-graphene composite material for selective laser sintering additive manufacturing," in Laser-Based Micro- and Nanoprocessing XVIII, (SPIE, 2024), pp. 317–324

Paper II: Laser-assisted processing of nano-graphite/silicon anode materials for improved performance of Li-ion batteries

Luke Bond, Henrik Andersson and Magnus Engholm

L. Bond, H. Andersson, and M. Engholm, "Laser-assisted processing of nano-graphite/silicon anode materials for improved performance of Li-ion batteries," in Laser-Based Micro- and Nanoprocessing XVIII, (SPIE, 2024), pp. 142–150

Paper III: Production of Yb:YVO₄ nanoparticles by pulsed laser ablation in liquid using a femtosecond laser

Luke Bond, Ellinor Jönsson and Magnus Engholm

L. Bond, E. Jönsson, and M. Engholm, "Production of Yb:YVO₄ nanoparticles by pulsed laser ablation in liquid using a femtosecond laser," in Laser Applications in Microelectronic and Optoelectronic Manufacturing (LAMOM) XXIX, (SPIE, 2024), pp. 74–81

Paper IV: Laser-formed nanoporous graphite anodes for enhanced lithium-ion battery performance

Luke Bond, Henrik Andersson, Magnus Hummelgård and Magnus Engholm

L. Bond, H. Andersson, M. Hummelgård, and M. Engholm, "Laser-formed nanoporous graphite anodes for enhanced lithium-ion battery performance," Applied Physics Letters 125(18), 181903 (2024)

List of acronyms

AM: Additive manufacturing

CW: Continuous wave

DI: Deionized water

DLS: Dynamic light scattering

EDS: Energy-dispersive x-ray spectroscopy

EV: Electric vehicle

LIB: Lithium-ion battery

LML: Laser melting in liquid

NG: Powder mixture of nanographite and graphene

NGSi: Composite powder consisting of a nanographite and graphene powder mixture with additional μm -sized silicon

NP: Nanoparticle

PA: Polyamide

PLAL: Pulsed laser ablation in liquid

RE: Rare-earth

SEM: Scanning electron microscopy

SLS: Selective laser sintering

1 Introduction

Since their inception in the 1960s, lasers have evolved into indispensable tools in various fields, including telecommunication¹⁻³, medicine⁴⁻⁸, manufacturing⁹⁻¹², and material science¹³⁻¹⁸. Their unique properties, such as coherence, monochromaticity, and high focus, make them ideal for precise energy delivery, offering exceptional control and efficiency in numerous applications. A key area of application is material processing, where lasers enable fine material modifications such as cutting^{19,20}, welding^{21,22}, surface treatments²³⁻²⁵, and nanoparticle (NP) synthesis^{14,26-28} with minimal waste. This versatility allows for the production of intricate designs and composites that are difficult to achieve with conventional methods.

Despite their advantages, challenges remain in using lasers for advanced functional material development, particularly where enhanced electrical, optical, or energy storage properties are required. Laser-assisted techniques offer a promising solution, enabling material structuring at the nano/micro-scale. This thesis explores these techniques for the development of next-generation materials, specifically focusing on three areas: polymer-graphene composites for conductive plastics, rare-earth (RE) doped NPs with controlled morphology, and laser-modification of a nanographite and graphene mixture (NG), as well as NG-silicon (NGSi) anode materials for lithium-ion batteries (LIBs). These developments not only demonstrate the potential of laser material processing, but also address key challenges in the fabrication of high-performance functional materials for emerging technologies.

1.1 Problem statement

The increased demand for advanced functional materials has heightened interest in laser-based material processing due to its ability to precisely control material properties. However, challenges remain in optimizing these processes for enhancing application-specific characteristics. For example, polymer-based selective laser sintering (SLS) typically uses non-conductive materials, limiting their utility in applications requiring electrical conductivity. The development of electrically conductive polymer composites via laser processing is still in early stages²⁹, requiring better process understanding for reliable performance.

Similarly, laser-assisted synthesis and modification of nanomaterials, such as RE-doped NPs and graphite-based anode materials for LIBs, face challenges in maintaining material stability, improving performance, and ensuring scalability^{26,30-32}. A deeper understanding of laser interactions with these materials is essential to optimize their structure and functionality, especially in enhancing LIB capacity and cycling stability.

1.2 Research objective

This research aims to develop and optimize advanced materials through laser-assisted processing for various applications. The focus is on three main areas: producing electrically conductive polymer-graphene composites for additive manufacturing (AM), enhancing LIB anode performance, and synthesizing RE-doped NPs that retain the bulk material's stoichiometry. The study explores scalable techniques, emphasising conductivity in composites, controlled NP synthesis via laser parameter selection, and LIB anode enhancement through laser structural modification.

1.3 Scope

This research focuses on developing advanced materials using laser-assisted processing for industrial and energy applications. It covers three main areas: electrically conductive polymer-graphene composites, LIB anodes, and RE-doped NP synthesis. SLS is used to create polymer-graphene composites with high electrical conductivity for electromagnetic compatibility. Laser-assisted processing of NG anodes aims to improve the capacity and stability of LIBs. Additionally, RE-doped NPs are synthesized via pulsed laser ablation in liquid (PLAL), with a focus on controlling their size, distribution, and maintaining stoichiometry with respect to the bulk crystal for photonics applications. The methodology addresses the following key research questions:

1. How will laser-assisted processing influence the conductivity and mechanical properties of a laser-formed polymer-graphene composite structure? – Paper I
2. How can laser-assisted processing be used to optimize the structure of graphite-based anode materials to improve the performance of LIBs? – Paper II/IV.
3. How will ultrashort pulses affect the structure and stoichiometry of synthesized RE-doped NPs? – Paper III

1.4 Thesis outline

This thesis explores laser material processing and its applications in developing advanced functional materials for energy storage, AM, and photonics.

In chapter 2 of this thesis, an overview of laser material processing is provided. It includes relevant laser theory, an introduction to different

laser systems and their applications, with a focus on functional materials, challenges, and related work in the field.

Chapter 3 describes the experimental setups used in this research. It covers both continuous wave (CW) and femtosecond laser (fs-laser) setups and the various characterization methods employed.

Chapter 4 presents the SLS of polymer-graphene composites. The production of conductive polymers, the choice of materials, and the laser parameters are discussed in detail, along with the effects of material structure and electrical resistance.

Chapter 5 focuses on laser processing of graphite-based anodes for LIBs. The performance improvements achieved through laser processing, such as increased porosity and better Si distribution, are explored, along with optimized laser parameters.

Chapter 6 details the synthesis of RE-doped NPs using fs-PLAL. It covers the effects of laser parameters on NP formation, morphology, and colloidal stability.

Chapter 7 concludes the thesis, summarising the findings and discussing the environmental, ethical, and societal impacts of the work. The chapter also outlines potential future research direction, and a section on the author's contributions.

The thesis concludes with a comprehensive bibliography.

1.5 Papers included in this thesis

Paper I focuses on producing conductive polymer-graphene composites for SLS. Resistance measurements and SEM analysis identified optimal parameters, achieving conductive structures with

low sheet resistance (1 k Ω /sq), suitable for electromagnetic compatibility. Increasing energy density reduced resistance overall, but results varied with scanning speed.

Paper II presents research focused on enhancing NGSi anode performance for LIBs. Laser processing reduced particle size and improved silicon distribution, confirmed by scanning electron microscopy (SEM) and energy dispersive x-ray spectroscopy (EDS). Higher intensity and slower scanning speeds in nitrogen minimized oxygen content. An improvement in capacity and stability was verified through cyclic voltammetry testing.

Paper III presents the synthesis of Yb:YVO₄ NPs via laser ablation in liquid, examining the effects of pulse rate and solvents. NP size and stability were influenced by pulse repetition and solvent choice (water vs. ammonia). Characterization with EDS and SEM showed consistent stoichiometry, with particle sizes ranging from 10 to 150 nm.

Paper IV presents research on NG anodes for LIBs, whereby nanoporous structures were formed via laser processing, confirmed with SEM and Raman spectroscopy. Battery testing, via galvanostatic charge-discharge and electrochemical impedance spectroscopy, demonstrated a >30% improvement in capacity at all charge rates.

2 Laser material processing

2.1 Introduction to laser material processing

The main interactions between light and matter are illustrated in Figure 2.1. Reflectivity is the optical property describing how light interacts with a material (Equation 2.1), influenced by factors such as refractive index and surface roughness.

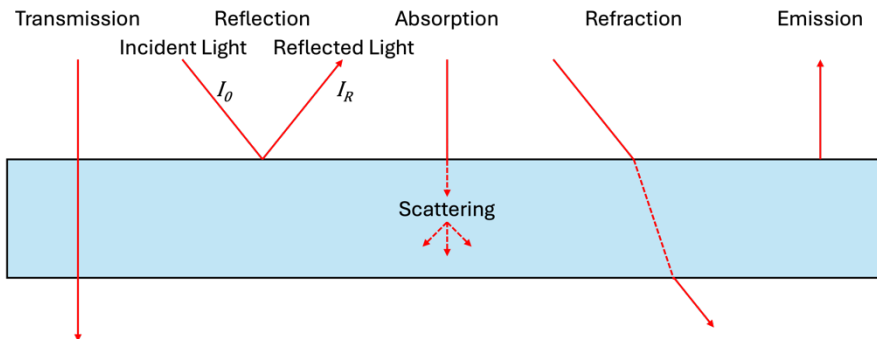


Figure 2.1 Main interactions between light and matter.

Equation 2.1: Reflectance of light R , where I_0 and I_R are the intensities of the incident light and reflected light respectively.

$$R = \frac{I_R}{I_0}$$

Equation 2.2: The intensity in the x-direction $I(x)$, incident light intensity I_0 , extinction coefficient κ , vacuum wavelength λ_0 , absorption coefficient α , and the penetration depth relationships $\frac{1}{\alpha}$.

$$I(x) = I_0 e^{-\frac{4\pi\kappa x}{\lambda_0}}, \quad \alpha = \frac{4\pi\kappa}{\lambda_0}, \quad \frac{1}{\alpha} = \frac{\lambda_0}{4\pi\kappa}$$

Absorption and penetration depth (Equation 2.2) depend on the wavelength of incident light λ_0 and material properties. Different

materials exhibit absorption peaks at specific wavelengths, as shown by Liu et al.³³, which can influence the efficiency and outcome of laser processing. This highlights the significance of selecting the optimal laser wavelength for the intended target material in laser material processing.

Equation 2.3 Laser fluence, F [J/cm^2], where E is the energy of the pulse [J], A is the area over which the energy is distributed [cm^2], I [W/cm^2] is the peak intensity, and τ is the pulse duration [s], typically at full-width half-maximum.

$$F = \frac{E}{A} = I \cdot \tau$$

As laser parameters are adjusted to optimize interactions, the absorbed energy directly influences the material's response. Once energy is deposited, the material's absorption coefficient and reflectivity play crucial roles in determining how effectively laser energy is converted to heat, and to driving processes such as melting, vaporization, or ablation³⁴. Laser fluence is defined in Equation 2.3. Heat distribution depends on substrate properties, with thermally conductive substrates dissipating thermal energy, while thermally insulating substrates retain it, concentrating heat in localized areas^{16,35}.

In metals, rapid localized heating reduces their reflectivity as temperatures rise³⁶, accelerating melting and enhancing energy deposition. Upon melting, optical properties such as reflectance and absorption can change significantly. For example, copper's reflectivity decreases while silicon's reflectivity increases³⁵, whilst still being wavelength-dependent. Additionally laser-induced plasma formation in steel sharply reduces reflectivity due to strong absorption by the plasma, which improves processing efficiency for reflective materials like metals under infrared and visible light laser radiation³⁵.

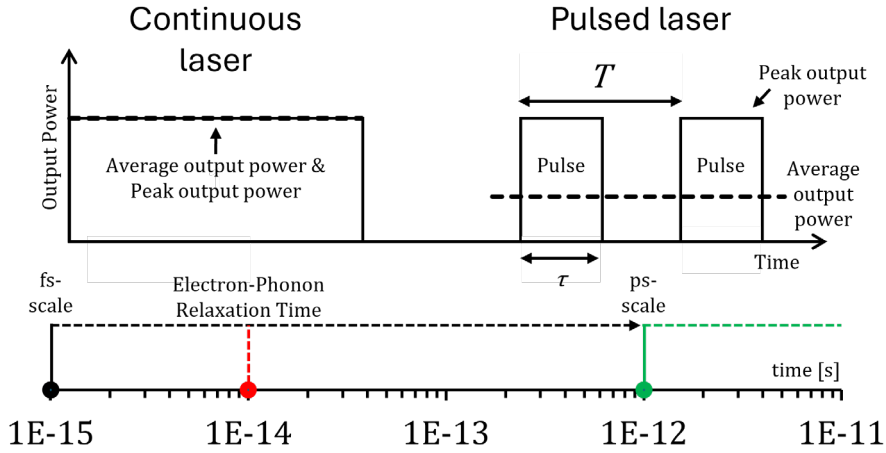


Figure 2.2 Comparison of continuous wave lasers versus pulsed lasers, where T refers to the time between the start of consecutive pulses, and τ refers to the duration of a pulse. The approximate magnitude of electron-phonon relaxation time, in this case for metals, is compared to the fs-scale and ps-scale for reference.

These changes in reflectivity and energy absorption depend on the mode of energy delivery in laser processing. In particular, the distinction between CW and pulsed lasers plays a crucial role (Figure 2.2). CW lasers provide constant energy over time, maintaining a steady beam intensity, as described by Equation 2.4. In contrast, pulsed lasers deliver energy in short bursts, enabling higher peak intensities, as shown in Equation 2.4.

Equation 2.4 Laser light intensity for CW and pulsed lasers, I [W/cm^2], where P is the power of the laser [W], and A is the area over which the energy is distributed [cm^2], and $P(t)$ is the instantaneous power at time t .

$$I = \frac{P}{A} (CW), \quad I(t) = \frac{P(t)}{A} (Pulsed)$$

Energy deposition in pulsed lasers is influenced by pulse energy, pulse duration, and the material's electron-phonon relaxation time τ_{ep} which represents how quickly energy is transferred from the excited electrons to the lattice (phonons) in a material. Shorter pulses, such as

those from fs-lasers, result in non-thermal effects, such as multiphoton absorption and Coulomb explosions, because energy deposition occurs faster than it can be dissipated through thermal conduction.

Equation 2.5 The rate of multi-photon ionization W , where $\sigma^{(k)}$ is the multiphoton ionization cross-section, I is the laser intensity, and k is the number of photons involved³⁷.

$$W = \sigma_{(k)} I^k$$

In the case of multiphoton ionization, where multiple photons are absorbed simultaneously, ionization rates follow Equation 2.5. Meanwhile, Coulomb forces drive material ejection (Equation 2.6) due to the rapid increase in charge density, minimising heat-affected zones³⁸.

Equation 2.6 Coulomb's law, where F is the electrostatic repulsive force between ions, where Z is the charge number of the ions, e is the elementary charge, ϵ_0 is the vacuum permittivity, and r is the inter-ionic distance.

$$F = \frac{Z^2 e^2}{4\pi\epsilon_0 r^2}$$

In contrast, nanosecond lasers, which have longer pulse durations, induce thermal effects such as melting and vaporization (Equation 2.7, Equation 2.8), resulting in larger heat-affected zones.

Equation 2.7: Energy required for vaporization Q , where m is the mass, c_p is the specific heat capacity, ΔT is the temperature rise, and L_v is the latent heat of vaporization.

$$Q = mc_p\Delta T + mL_v$$

Equation 2.8: Vaporization laser fluence threshold F_v , where Q_{abs} is the energy absorbed, and A is the irradiated area.

$$F_v = \frac{Q_{abs}}{A}$$

Plasma formation may occur at high fluence, affecting laser-material interaction based on electron density (Equation 2.9).

Equation 2.9: The plasma frequency ω_p , where N_e is the electron density, e is the elementary charge, ϵ_0 is the vacuum permittivity, and m_e is the electron mass.

$$\omega_p = \sqrt{\frac{N_e e^2}{\epsilon_0 m_e}}$$

When electron density exceeds a critical threshold, the plasma either reflects or absorbs laser light, depending on whether the plasma frequency is higher or lower than that of the incident light. This can shield the material, reducing laser interaction, or enhance material removal via shockwaves.

The efficiency and effectiveness of laser material processing is further dependent on interrelated laser parameters such as scanning speed, spot size, pulse repetition rate, and pulse overlap. Dwell time (Equation 2.10) and average power (Equation 2.11) control energy accumulation, with pulse overlap enabling cumulating heating (Equation 2.12)

Equation 2.10: Dwell time t_{dwell} , where d is the spot size, and v is the scanning speed.

$$t_{dwell} = \frac{d}{v}$$

Equation 2.11: Average power of a pulsed laser P_{avg} , where E is the pulse energy, and f is the repetition rate.

$$P_{avg} = E \cdot f$$

Equation 2.12: The degree of overlap OD (in per cent), where t_{dwell} is the dwell time, and f is the pulse repetition rate.

$$OD = \left[1 - \frac{1}{f \cdot t_{dwell}} \right] \cdot 100, \quad \text{for } \frac{1}{f} \leq t_{dwell}$$

$$= 0, \quad \text{for } \frac{1}{f} > t_{dwell}$$

Here, overlapping of multiple successive shorter pulses can prevent complete cooling, pushing the material modification mechanism from non-thermal effects, such as Coulomb explosions and multiphoton ionization, to thermal processes in the case of using fs-pulses.

Overall, thermal (Photothermal) effects cause melting and/or vaporization, while non-thermal (photochemical) processes involve molecular changes without significant heating. High peak intensities from pulsed lasers can break bonds or induce reactions at specific fluence thresholds.

2.2 Types of laser systems

Lasers come in various types, each with unique characteristics tailored to specific applications. A summary of key types of laser systems is provided in Table 2.1.

Table 2.1 Types of laser systems, information acquired from³⁵.

Laser Type	Light Source	Advantages	Disadvantages	Typical Use Cases
Fiber	Optical fibers, doped with RE elements	Compact design, high efficiency, excellent beam quality	Higher initial cost, heat management challenges	Metal cutting, welding, medical applications, telecommunications
Solid-state	Solid gain medium (e.g., Nd, Ruby, Ti)	High power output, good beam quality, application versatility	Bulkiness for high-power version, higher operational cost	Laser cutting, welding, medical applications, microfabrication
Gas	Gas medium (e.g., CO ₂ , HeNe, excimer)	High power output, good for large-area processing.	Large size, requires gas replenishment, may have lower efficiency than solid-state lasers	Cutting, engraving, medical (laser surgery), scientific applications
Semi-conductor	Semiconductor diodes (e.g., GaAs)	Cost-effective and compact, high efficiency	Limited power output, reduced beam quality	Fiber optic communication, barcode scanners, laser pointers,

2.3 Laser applications in material processing

Laser applications in material processing are extensive, offering enhanced precision, efficiency, and versatility across manufacturing. Macro-scale processes include cutting, welding, cladding, alloying, drilling and brazing, while micro-scale processes include micro texturing, scribing (referring to the production of perforation lines which separates a large controlled amount of material via laser ablation), and micro drilling^{17,39}. Standard laser processes, such as cutting, welding and drilling have reached market maturity⁴⁰ with their fine focus enabling precise cuts and holes and minimalizing material waste¹⁶. Furthermore, lasers also offer a non-contact solution for challenging materials, reducing mechanical stress and damage³⁹.

Additionally, lasers play a crucial role in AM, especially in sintering. They selectively heat powdered materials to fuse particles without fully melting them, enabling the production of complex geometries with minimal waste^{18,41}. This technique reduces post-processing and enables the creation of lightweight, optimized structures, without the need for incorporated support structures.

2.4 Challenges and opportunities

Laser material processing has revolutionized manufacturing and research, offering precision, efficiency, and versatility. However, challenges remain, particularly when scaling from laboratory setups to industrial production. Maintaining uniformity and consistent quality, especially with complex materials, poses difficulties, and high initial costs hinder widespread adoption. Furthermore, not all materials absorb laser energy efficiently, leading to unpredictable outcomes, especially in composites. Managing thermal effects is also critical to avoid material damage, even with advanced pulsed lasers.

Despite these challenges, advancements in laser technologies, such as fiber and ultrafast lasers, hold promise for improving scalability and reducing costs. The integration of automation and artificial intelligence can optimize processes in real-time, ensuring consistent quality. Innovations in thermal management, like micro-channel cooling^{42,43}, address heat-related issues, enhancing precision.

Future development in laser processing, including applications in energy storage^{23,44,45}, additive manufacturing^{18,29,46}, and nanotechnology^{4,26,47}, will enable complex structures with high precision. Sustainable practices, like energy-efficient systems and eco-friendly materials, will further drive innovation in this rapidly evolving field.

2.5 Related work

Given the broad range of scientific fields involved in the various applications of laser-processed materials presented in this thesis, there is an extensive body of related work.

Electrically conductive polyamide (PA) 12/graphene structures via SLS have been previously demonstrated by Meng et al.⁴⁶ and Chen et al.⁴⁸, while Navik et al. reported a scalable production method for PA6/graphene composites with enhanced electromagnetic shielding at a maximum graphene loading of 3 wt.%⁴⁹. Additionally, Rollo et al. successfully fabricated porous 3D conductive structures using thermoplastic polyurethane powder coated with multi-walled carbon nanotubes and graphene nanofillers⁵⁰. However, previous studies on PA11/graphene nanoplatelets for SLS, with loadings up to 5 wt.%, showed inadequate graphene dispersion within the matrix, limiting improvements in thermal stability and electrical conductivity⁵¹.

Moreover, studies on optimizing laser parameters to enhance the electrical conductivity of polymer-graphene composites remain scarce.

In the field of energy storage, graphite is widely utilized as an anode material⁵². Strategies to increase surface area, such as using carbon-based nanostructures, as discussed by Roselin et al.⁵³, employing potassium hydroxide etching to create pore/hole structures, as demonstrated by Kim et al.⁵⁴, or applying perchloric acid with heat treatment to increase d-spacing to form expanded graphite as shown by Lee et al.⁵⁵, have been shown to enhance lithium-ion diffusion, prevent structural degradation, and improve electrochemical performance in the anode. Additionally, the use of Si, with a theoretical specific capacity of 4200 mAh/g, has been widely reported as a possible avenue for improving energy density in LIBs^{31,32}. However, the mechanical degradation of Si particles during charge-discharge cycles^{32,56}, remains a challenge. Potential solutions, such as using Si NPs as discussed by Feng et al.⁵⁷ and incorporating Si within a graphite matrix as demonstrated by Sehrawat et al.³¹, have shown promise in mitigating issues related to silicon's mechanical stability. On the other hand, the synthesis of Si NPs is typically associated with environmental issues and high costs, whilst Kabashin et al. has indicated that laser pyrolysis processes have been scaled to kg/h volumes²⁸.

In relation to direct laser material processing of graphite-based anode materials, Qian et al.⁵⁸ demonstrated a correlation between laser fluence and the formation of various carbon phases, while Khosla et al.²³ reported enhanced LIB capacity and performance through nanosecond-pulsed laser annealing by controlling surface defects and microstructure. Additionally, Alhajji et al.⁵⁹ achieved improved capacity and rate performance by synthesizing laser-induced

graphene on various carbon sources. The production of 3D LIBs with periodic structures via laser structuring has also been shown to improve rate capability^{44,45,60}. However, to the best of this researcher's knowledge, the use of laser processing to transform μm -scale graphite and Si into a porous matrix, while simultaneously reducing particle size, has not yet been reported.

Regarding photonics and RE-doped NPs, Du et al.²⁷ discusses a variety of lanthanide-activated NPs synthesized via PLAL. Focusing on Yb:YVO₄ NPs, Wang et al.^{61,62} successfully demonstrated the synthesis of YVO₄:Eu³⁺ using ns-PLAL, obtaining ovoid-like structures in deionized (DI) water, and spherical structures in ethanol. However, some asymmetry around the europium ions was observed, suggesting a loss in stoichiometry. Hybrid RE-doped optical materials, which embed RE-doped NPs into hosts with advantageous properties like silica, are emerging for enhanced spectroscopic performance in photonics. Recent advancements include the successful incorporation of YbPO₄ NPs in as-drawn silica fibers by Lu et al.⁶³, maintaining their crystal structure and offering promise for similar materials, such as Yb:YVO₄. To date, the synthesis of Yb:YVO₄ NPs via laser ablation in liquid is unexplored, especially using fs-laser ablation, as is the challenge of achieving Yb:YVO₄ NPs with stoichiometry matching that of bulk material.

3 Experimental

This chapter outlines the laser systems utilized, as well as the characterization methods employed throughout this research.

3.1 Laser setups

The CW laser setup (Figure 3.1) consists of a 1064 nm CW fiber laser, connected to a galvanostatic SCANLAB mirror scanner (placed on a y-axis mount within acrylic housing with a ventilation system), producing a spot size of 60 μm . The scanner is connected to a control box, utilising the E1701D modular XY2/100 scanner controller, and controlled via laser marking software (BeamConstruct, HALaser Systems).



Figure 3.1 Photo of CW laser setup.

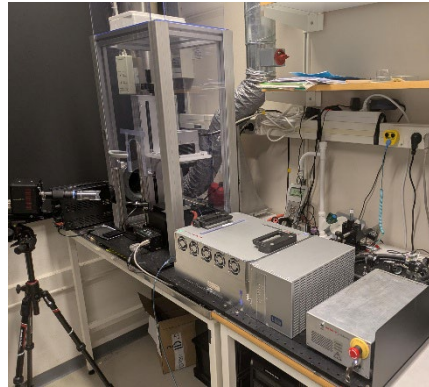


Figure 3.2 Photo of fs-laser setup.

The fs-laser system (Figure 3.2) consists of a 1030 nm femtosecond laser (NKT Photonics, ORIGAMI XP10 free-space, 350 fs pulse duration) coupled to a SCANLAB mirror scanner (placed on a y-axis mount within acrylic housing with a ventilation system) producing a spot size of 40 μm , and controlled by EZCAD2 laser marking software. A thorLABS motorized lab jack with y-translation is utilized, allowing

for simple system height adjustments without adjusting the entire mirror-lens setup.

3.2 Characterization methods

The characterization methods employed across all projects include SEM imaging to analyse surface morphology and microstructure, offering insights into the material's properties after laser processing. Elemental analysis through EDS was also performed to assess the distribution and composition of elements within the samples. Dynamic light scattering (DLS) and zeta potential measurements were used in production of Yb:YVO₄ NPs to evaluate colloidal size distribution and stability, ensuring that the particles remained well-dispersed in solution, while Raman spectroscopy verified the structural integrity of the NPs by comparing their spectra to the bulk Yb:YVO₄ crystal. For the polymer-graphene composites, 2-point resistance measurements were conducted to determine sheet resistance.

In the laser-processed nano-graphite/Si anode materials, standard CR2032 coin cells were assembled using the anode material and lithium metal as the counter electrode. Cyclic voltammetry was conducted to evaluate redox reactions and capacitance variations. Electrochemical impedance spectroscopy was used to assess ion diffusion and charge transfer resistance, while galvanostatic charge-discharge testing was performed to measure specific capacity and cyclability. X-ray diffraction spectroscopy was also utilized to examine changes in the d-spacing of the graphite lattice following laser processing.

4 Selective laser sintering of polymer-graphene composites

The demand for electrically conductive plastics has grown due to the need for electromagnetic compatibility, particularly in electric vehicles (EV), where shielding from electromagnetic interference is crucial. Conductive polymers combine the flexibility of plastics with electrical conductivity, enabling applications such as flexible electronics, sensors, and conductive enclosures.

Additive manufacturing (AM), especially powder bed fusion, supports the production of high-resolution, complex parts while minimizing material waste. SLS, a key subset of powder bed fusion, uses lasers to fuse polymer powders layer by layer, producing detailed 3D objects without molds.

This research aims to leverage SLS to produce electrically conductive polymer composites by integrating graphene into a polymer matrix. Graphene's excellent electrical conductivity, mechanical strength, and potential for renewable production, make it a promising additive. Polyamide 11 (PA11), a commonly used polymer in SLS, was chosen as the base material for this investigation.

The following sections will explore the SLS process, the characteristics of PA11, and the optimal parameters for producing conductive polymer-graphene composites, focusing on how the sintering process affects the material's structure and electrical properties.

4.1 Selective laser sintering

SLS is an AM technique using a laser to sinter powdered materials, creating solid structures layer by layer^{18,41}. Powder is spread on a

platform, and a laser selectively heats areas just below the melting point, fusing particles. After each layer solidifies, a fresh powder layer is added, repeating the process. SLS stands out among AM methods for its capability to process a range of materials, including polymers, metals, and ceramics, without requiring support structures^{18,41,46}. This versatility is due to the surrounding unsintered powder that stabilizes each layer as it builds. Compared to other AM methods like stereolithography, which only works with photopolymers and offers very high resolution, and fused deposition modelling, known for low-cost, multi-material printing but anisotropic properties, SLS produces parts with high strength and chemical resistance¹⁸.

Polyamide 11 (PA11) is widely used in SLS due to its durability, flexibility, and resistance to various chemicals⁶⁴. As a bio-based material derived from castor oil^{65–67}, it offers a more sustainable option compared to petroleum-based alternatives like PA12^{64,68}. Furthermore, PA11 is a semi-crystalline thermoplastic with good flowability and favourable sintering behaviour, which results in devices with good mechanical properties⁶⁹.

4.2 Conductive polymers and selective laser sintering

Conductive polymers are increasingly important in industries like electronics and aerospace for their lightweight, electrically conductive properties^{41,46,70}. SLS allows the incorporation of conductive fillers, such as graphene, into polymers, creating composites that combine electrical conductivity with mechanical strength^{46,71,72}. Achieving the percolation threshold, the minimum filler concentration required to form a conductive network⁷², is a key challenge. SLS requires precise

control over laser and material parameters for optimizing filler distribution and enhancing material performance^{41,72-74}.

Graphene, a single layer of carbon atoms with exceptional electrical, mechanical, and thermal properties, stands out as a superior conductive filler⁷⁵⁻⁷⁷. For graphene-based composites, the percolation threshold has been demonstrated to be as low as 0.2% by weight, for electrically conductive parts, by Meng et al.⁴⁶, with conductivity further rising with increase conductive filler content⁷⁸. Additionally, graphene reinforces mechanical properties such as tensile strength and flexibility^{46,48}, making it a versatile option for applications that demand durability and electrical performance. Moreover, graphene's potential for being sourced from renewable materials adds an environmental benefit^{77,79}.

4.3 Fabrication of conductive polymers via selective laser sintering

The choice of laser for SLS depends on the target material's absorptivity, which varies across materials⁷¹. The 1064 nm CW fiber laser is particularly suitable for polymer-graphene composites, interacting efficiently with both PA11 and graphene⁸⁰, as well as being a typical wavelength utilized in desktop SLS printers⁸¹. Additionally, the CW laser's continuous energy delivery ensures even thermal distribution, lowering defects with reduced thermal gradients⁸² and improving interparticle bonding, essential for electrical conductivity. Graphene's high thermal conductivity⁸³ further aids in efficient heat transfer, promoting effective melting and bonding of PA11 particles. In contrast, pulsed lasers induce rapid heating and cooling, creating localized hot spots and enhancing directional texturing⁸².

4.4 Laser parameter selection and optimization

The research on SLS of PA-graphene composites was conducted with a focus on optimizing laser parameters and their effect on material structure and resulting electrical conductivity. Initial testing consisted of producing in-house powder mixtures of various forms of graphene with PA11 powder and performing oven melt mixing in the temperature range of 200-270 °C for up to 10 minutes. The forms of graphene utilized consisted of graphene powder (GP5, 2dFab), edge-oxidized graphene (Sigma Aldrich), and graphene oxide (2dFab). Loadings of 1-5% by weight were utilized for each sample. However, all samples exhibited resistance values exceeding the measurement range of the multimeter (overload), indicating that a conductive network did not form under oven processing conditions, possibly due to agglomeration and localization of graphene flakes.

Graphene-based coatings with a loading of 0.5% and a wet thickness of 200 μm were applied to photopaper using a 4-sided film applicator. The coatings varied in number of layers, using edge-oxidized graphene and graphene oxide samples with and without the use of TX-100 surfactant as binder. However, difficulties surrounding the laser processing of edge-oxidized graphene samples resulted in very limited, in-conclusive, resistance measurements and will therefore not be considered. Graphene-oxide coatings were produced with 9 (GO9) and 20 (GO20) layers, whilst graphene-oxide and PA11 coatings were produced with 10 (GOPA10) layers only. Here, laser processing was performed on each sample through a range of energy density values, with either 1 or 2 loops. Noticeable correlations between samples are the decrease in sheet resistance with both increasing energy density

values, as also demonstrated in paper I, and an increase from 1 to 2 loops as seen in Figure 4.1

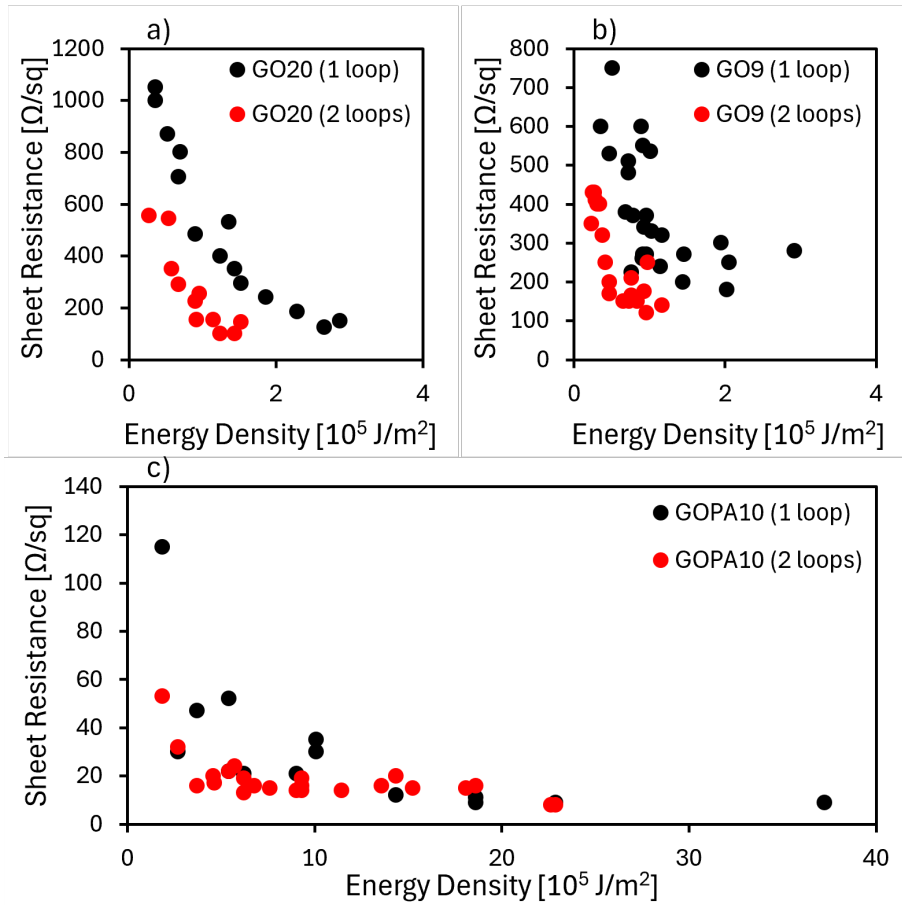


Figure 4.1 Energy density vs sheet resistance values following laser processing with 1-2 loops for a) graphene oxide coating with 20 layers (GO20), b) graphene oxide coating with 9 layers (GO9), and c) graphene oxide polyamide composite coating with 10 layers (GOPA10). Sheet resistance was calculated via 2-point resistance measurements of a 3 mm x 3 mm area.

Furthermore, it appears that an increase in the number of layers from GO9 to GO20 led to a stronger correlation between energy density and sheet resistance, likely due to sample degradation with reduced

thickness for heat distribution during laser processing. However, within the range of energy densities utilized, it appears that both GO9 and GO20 reach a minimum resistance around 100 Ω/sq regardless of number of layers. With the addition of PA11 into the coatings, the GOPA10 sample is noticeably able to withstand significantly higher energy density values during laser processing. Once again, the same correlations regarding energy density and loops are observed in the resulting sheet resistance, however reaching a significantly decrease plateau around 9 Ω/sq . Such a difference in applicable energy densities during laser processing may further be explained by weight measurements of the samples, as shown in Table 4.1.

Table 4.1 Minimum sheet resistance values for graphene oxide-based coatings (GO9, GO20, and GOPA10), with their given area weight.

Sample	Coating Weight [g/m ²]	Sheet Resistance [Ω/sq]
GO9	7	120
GO20	10	100
GOPA10	72	8

PA11-graphene composite powder with 4% weight loading (2dFab) was obtained for SLS, and performed in Paper I. The composite powder was determined to consist of PA11 particles coated with graphene flakes, with displayed variations in conductivity due to inconsistencies in graphene coverage. Imperfection in the graphene network likely caused these variations, with some regions showing incomplete coverage.

The PA11-graphene composite powder was pre-heated on a hot plate at 170°C to reduce the required energy input for sintering, minimising thermal damage and preserving the integrity of the composite during laser exposure. Excessive melting, caused by high energy densities, resulted in plasticization and deformation due to the large energy input. In contrast, lower energy inputs led to incomplete material fusion, as demonstrated by SEM imaging in paper I. Structural voids were observed in insufficiently sintered regions, linked to powder density and the flow of graphene material, highlighting the need for fine control over laser parameters and pre-heating processes. Cross-sectional SEM imaging in paper I further revealed insights into how laser energy may have been distributed throughout the depth of the PA11-graphene composite. Sintering and melting effects were largely confined to the top layers, where most of the energy was absorbed, while the lower layers remained partially fused, indicating that achieving uniform heat distribution across the entire material depth remains a challenge.

Conductivity was indirectly determined via 2-point resistance measurements of the resulting PA11-graphene solid structure. The sheet resistance was found to be closely linked to the degree of sintering and plasticization of the formed structure. Increasing plasticization correlated with higher sheet resistance, with overloaded resistance values recorded in fully plasticized structures. On the other hand, optimized energy density paired with appropriate scanning speeds, as demonstrated in paper I, led to improved sintering, reducing resistance and resulting in a more conductive structure with resistance values ranging from 1-8 kΩ/sq. Paper I further explores the relationship between laser light intensity [kW/cm²] and scanning speed [mm/s] on sheet resistance, showing that energy density alone is

insufficient to fully estimate sheet resistance due to the complex laser-material interactions in SLS. Key factors such as laser intensity, scanning speed, interline distance, and spot size therefore play a critical role in ensuring uniform energy delivery and heat distribution, and determining the quality of the sintering process.

5 Laser processing of graphite-based anodes

5.1 Lithium-ion batteries

LIBs function through the movement of Li-ions between the anode and cathode during charge and discharge cycles. These electrodes are separated by a liquid electrolyte, which facilitates ion movement, and a separator that prevents direct contact between the anode and cathode, protecting against short-circuits in the case of electrolyte evaporation. Anode materials are typically tested in a half-cell format, utilizing lithium foil as the counter electrode, whereby Figure 5.1 indicates the assembly order for coin cells used in this work.

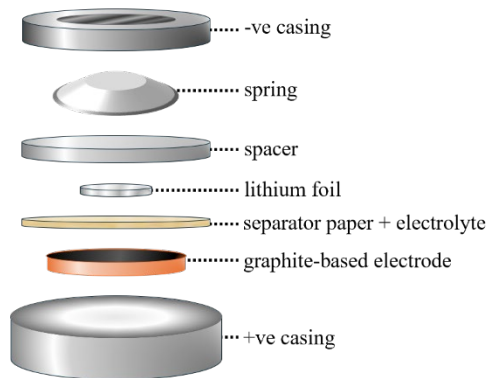


Figure 5.1 Coin cell assembly for graphite-based anode materials, in a half-cell format.

5.2 Graphite anodes

Graphite is the most widely used anode material in LIBs due to its high theoretical capacity of 372 mAh/g, low lithiation voltage (0.1 – 2 V vs. Li/Li+), and stable performance across numerous charge cycles. These attributes make it ideal for applications like EVs and portable

electronics, which demand high energy density, long cycle life, and reliable performance. Graphite also exhibits good electrical conductivity and structural stability, ensuring efficient electron transport and minimal volume changes during Li-ion intercalation, while its thermal stability allows safe operation at varying temperatures. Its abundance and low cost make it practical for large-scale production, fulfilling the performance and economic requirements for LIBs in these industries.

Efforts to improve graphite's performance involve structural modifications, such as producing periodic structures^{44,45,60}, incorporating nanographite^{84,85}, graphene^{86,87}, or carbon nanotubes^{88,89}. These modifications increase surface area, porosity, and the number of active sites for Li-ion intercalation, improving diffusion and preventing structural degradation. This enhances cycling stability and specific capacity, which is critical for high-demand applications like EVs.

While Si offers much higher theoretical capacity (up to 4200 mAh/g), its significant volume changes during cycling lead to mechanical degradation. To mitigate these issues, the use of nano-Si is being explored^{32,56}, which exhibits reduced mechanical stress due to its smaller size, enabling improved structural integrity during cycling. Furthermore, the challenge of silicon's low conductivity can be addressed by integrating conductive additives, such as active carbon or carbon black, to enhance electron transport^{32,90}.

A promising approach involves embedding nano-Si within a graphene or nano-graphite matrix³¹. The conductive properties of graphene or graphite not only improve overall conductivity but also provide mechanical support, helping to accommodate silicon's volume

expansion during cycling. This synergistic composite approach leverages the high capacity of Si while maintaining structural integrity and enhancing charge transfer capabilities. Furthermore, exploring low-cost approaches, such as utilizing micro-sized Si and nanographite, followed by cost-effective processing methods for size reduction, can significantly improve performance while keeping manufacturing expenses low, which is required for large-scale adoption. Ongoing research focuses on refining these strategies to maximize the specific capacity of graphite-based anodes while effectively addressing the challenges associated with Si integration.

5.3 Electrode material refinement

A 1064 nm CW laser was used as a heat source for processing low-cost graphite-based anodes, including NG and a NGSi composite. This wavelength is well-suited for both graphite⁸⁰ and Si⁹¹ due to their absorption properties. While silicon's higher transmittance in the near-infrared can limit laser absorption, graphite's high thermal conductivity assists in the distribution of thermal energy for homogeneous laser processing of the material.

Laser processing induces localized heating, leading to the vaporization of graphite and Si particles upon reaching their respective vaporization thresholds, reducing them to the nanoscale and increasing material porosity. This porosity is critical for improving Li-ion intercalation by providing more active sites for lithium storage and enhancing ion transport. Additionally, forming a graphite-Si matrix structure enhances mechanical stability and overall anode performance. Unlike high-temperature ovens typically used for NP production, laser processing offers precise control over temperature and processing

conditions, optimizing structural properties and electrochemical performance of the anodes.

5.4 Optimization of laser parameters

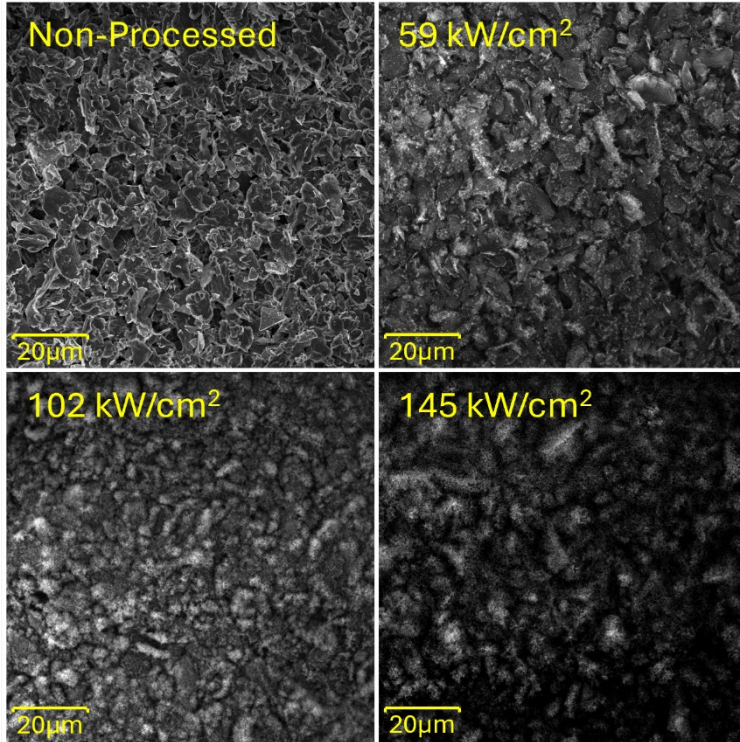


Figure 5.2 Effect of laser light intensity on NGSi electrodes (controlled variables: 50 mm/s, 5 loops).

The research conducted on the laser processing of low-cost graphite-based anodes, specifically NG and NGSi composites, revealed the significant impact of various laser parameters on their structural and electrochemical properties. Key observations highlighted the importance of laser light intensity, scanning speed, interline distance, and processing atmosphere in achieving the desired particle size reduction to the nanoscale. Higher laser light intensity enhanced material removal and promoted structural modifications (Figure 5.2),

while slower speeds facilitated increased energy absorption, porosity, and Si distribution in the resulting structure as discussed in paper II.

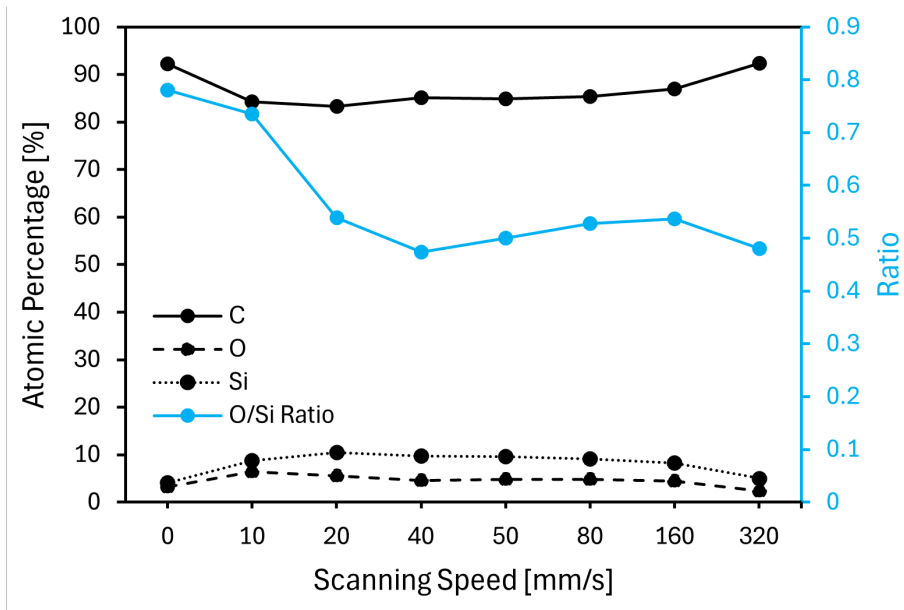


Figure 5.3 EDS of NGSi following laser processing in nitrogen atmosphere at a laser light intensity of 145 kW/cm² with scanning speeds ranging from 0 mm/s (non-processed) to 320 mm/s. Shown are the atomic percentages of carbon (C), oxygen (O), and silicon (Si), with the blue line and axis representing the representative ratio of O/Si.

However, optimizing laser parameters based on final material morphology and porosity also resulted in decreased silicon-to-oxygen ratios, as shown in Figure 5.3. Here, it is evident that the applied laser parameters of 145 kW/cm² at 20 mm/s for a single repetition, in paper II, resulted in increased O/Si ratios compared to higher scanning speeds, whilst continuing to maintain a lower O/Si ratio compared to non-processed and 10 mm/s. On the other hand, Si content was maximized alongside the advantages previously discussed when applying these laser parameters. Additionally, the interline distance

was determined in relation to the laser spot size, contributing to homogeneous processing and maintaining structural integrity.

The atmosphere during laser processing also influenced the properties of the graphite-based anodes. Processing under ambient conditions introduced oxidation reactions that reduced carbon content and affected Si oxide formation, as shown by increased O/Si ratios in Figure 5.4 with increased laser energy deposition.

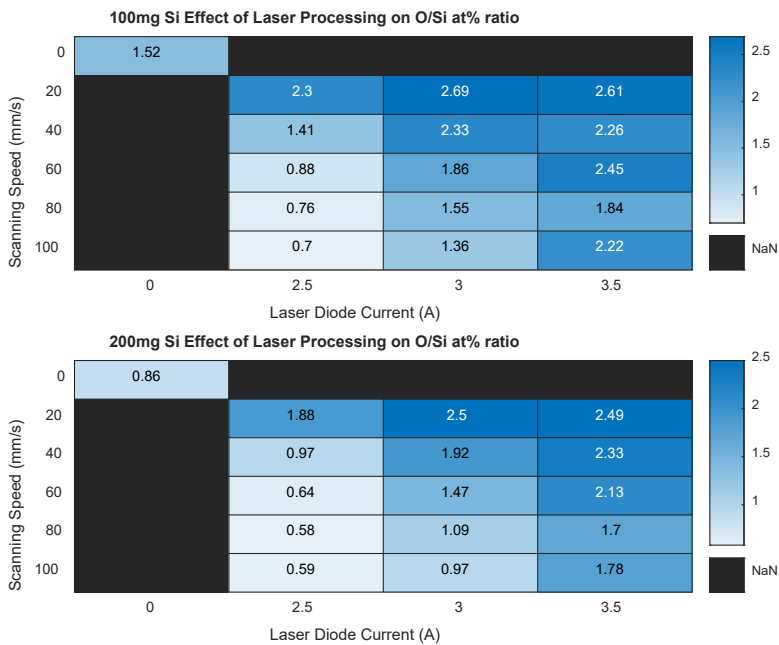


Figure 5.4 Effect of laser processing on O/Si atomic weight percentage (at%) ratio (obtained via EDS) in ambient atmosphere. The top-left value represents the non-processed material. 100 mg and 200 mg refers to the amount of silicon included in each coating slurry respectively.

In contrast, using an inert atmosphere, such as nitrogen, minimized these reactions and maintained the crucial balance between Si, oxygen, and carbon observed in paper II.

Size reductions to the nanoscale, as well as significantly increased porosity, were observed in both graphite-based anodes following laser processing. Structural changes observed in the NG anodes included increased surface defects, with nanoscale size reduction, and a transition to a more amorphous state, as verified by essentially identical X-ray diffraction spectra for the bulk material (Figure 5.5) and identification of the porous surface layer as amorphous carbon via Raman spectroscopy in paper IV. These structural transformations significantly contributed to the enhanced porosity. In the NGSi anodes, laser processing also achieved nanoscale size reduction alongside a more uniform distribution of Si within the graphene matrix, shown in paper II.

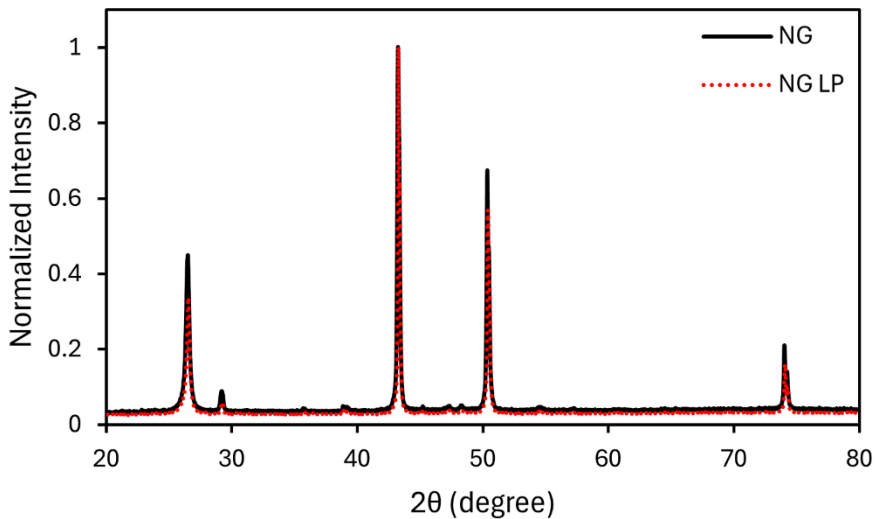


Figure 5.5 X-ray diffraction spectra of laser-processed and non-processed NG electrodes.

The performance of the resulting batteries demonstrated significant improvements, with the laser-processed NG anodes exhibiting enhanced charge/discharge rates and overall capacity retention

compared to unprocessed materials in paper IV. The NGSi anodes further benefited from the synergistic effects of both materials, resulting in improved reaction kinetics and the inclusion of additional Si features compared to their non-processed counterparts, determined in paper II.

The principles of laser theory shed light on the observed results. High-energy laser light generates localized heating, producing high temperatures that caused bond-breaking and structural disorder within the graphite. This localized energy induced a transition from crystalline graphite to a more amorphous structure via vaporization of carbon, enhancing porosity, increasing Li-ion intercalation sites, and promoting faster ion transport for NG in paper IV. In the case of the NGSi anodes in paper II, the localized heating led to vaporization and subsequent redistribution of Si NPs across the composite matrix.

6 Synthesis of rare earth-doped nanoparticles via laser

6.1 Pulsed laser ablation in liquid

PLAL offers a promising route for synthesizing nanomaterials, allowing for precise control over size and morphology, often resulting in high-purity NPs^{14,92}. This process involves the use of high-power lasers to ablate bulk material within a liquid medium, breaking it down into NPs. NP formation relies on both the physical disintegration of the bulk material and the chemical interactions between the ablated species and the surrounding liquid.

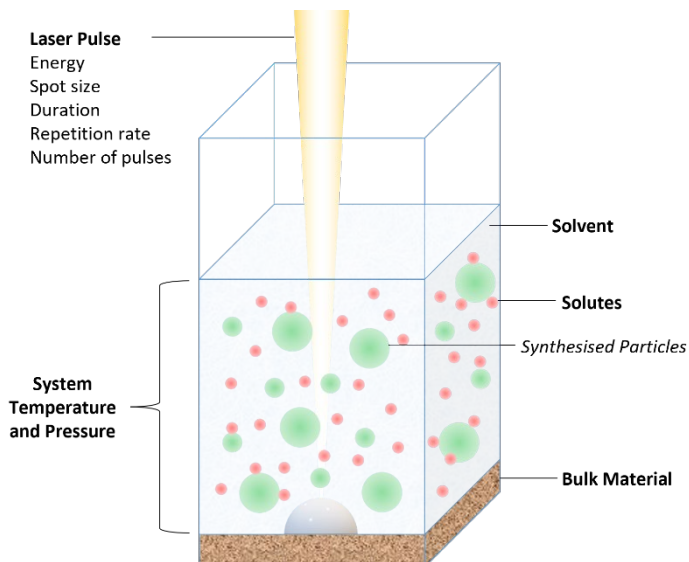


Figure 6.1 The main experimental parameters of PLAL: laser, bulk, and solvent parameters.

The mechanism begins with a laser pulse penetrating the liquid and being absorbed by the bulk material, triggering the material's ejection

via ablation. The resulting plasma plume, rich in ionized species, expands and cools rapidly within the liquid. As the plasma dissipates, the energy released from the plasma to the liquid initiates the formation of a cavitation bubble, which undergoes expansion and subsequent collapse, emitting a shockwave. This shockwave helps finalize the NP size and morphology by breaking larger fragments into smaller NPs. At this stage, if the NP dispersion is not stable, agglomeration may occur, and surface oxidation is possible based on the NP composition and liquid environment.

Laser parameters, such as pulse duration, fluence, and wavelength, play a pivotal role in determining the properties of the ablation process. Shorter pulses, such as fs-pulses, primarily cause non-thermal effects⁴⁷, resulting in fragmentation of the target material⁹². In contrast, ns-pulses lead to thermal effects, producing melted droplets, which are ejected from the target and can undergo further vaporization⁹². Higher laser fluences generally increase overall productivity⁹³ but can also lead to larger particle sizes with a broader size distribution^{92,94}. The wavelength must be carefully selected to match the absorption characteristics of the material, ensuring efficient energy transfer⁹⁵.

The choice of solvent is equally crucial, as it significantly affects the NP size and structure. Solvent properties, such as viscosity⁹⁶, density⁹⁷, and surface tension⁹², influence the dynamics of the cavitation bubble and the confinement of the plasma plume. Increased viscosity and density enhance the confinement, improving ablation efficiency⁹⁷. Moreover, solutes or surfactants added to the solution can cap the NP size by adsorbing onto the particle surface, preventing further growth and reducing agglomeration^{92,98}. These solutes may also chemically interact with the ablated material, forming compounds that differ from the bulk material.

Lastly the bulk material itself influences the NP formation. The ablation threshold, thermal conductivity, and optical absorption characteristics of the target material dictate how efficiently it can be ablated. Materials with high absorption at the laser wavelength and lower thermal conductivity typically produce finer NPs, as they facilitate rapid heating and localized melting, rather than extensive thermal diffusion⁹⁹.

6.2 Selection of target material for pulsed laser ablation in liquid

Yb:YVO₄ is a widely used crystalline material in solid-state lasers and various applications due to its efficient optical properties and robust performance¹⁰⁰. It effectively incorporates Yb³⁺ ions, which have a simple two-level energy structure¹⁰¹, allowing for more efficient laser operation with minimal heat generation and higher power output due to their low quantum defect¹⁰². Yb:YVO₄ exhibits high absorption efficiency around 985 nm, and could have promising applications for efficient diode-pumped solid-state lasers¹⁰².

The YVO₄ host crystal is notable for its excellent thermal conductivity, mechanical strength, and high optical damage threshold, ensuring stability in high-power laser systems¹⁰⁰. Additionally, Yb:YVO₄ is transparent in both the visible and near-infrared regions, further enhancing its utility in laser applications.

6.3 Choice of laser system

There are many factors which contribute to the laser system selected. Notably, there is a lack of research surrounding ultrafast PLAL of RE-doped bulk materials. Furthermore, previous articles which synthesized Yb:YVO₄ NPs via ns-PLAL in both ethanol and water

indicated stoichiometries which were unlike the bulk target material^{61,62}. Additionally, Yb:YVO₄ is a near-transparent crystal with a specific absorption peak around 980 nm. By utilising a fs-laser system, the low absorption values of Yb:YVO₄ become less important due to multi-photon absorption due to the laser light intensity exceeding 10⁸ [W/cm²]³⁵, allowing for efficient ablation, also dependent on solvent choice. In this case, two liquids were investigated: DI water and 5% ammonia solution.

6.4 Synthesis of Yb:YVO₄ nanoparticles

In this research on fs-PLAL of Yb:YVO₄ crystals, laser parameters played a fundamental role in shaping the morphology and characteristics of NPs. The intensity of the fs-pulses, pulse energy, repetition rate, focal point, and ablation time all had significant effects on the ablation process.

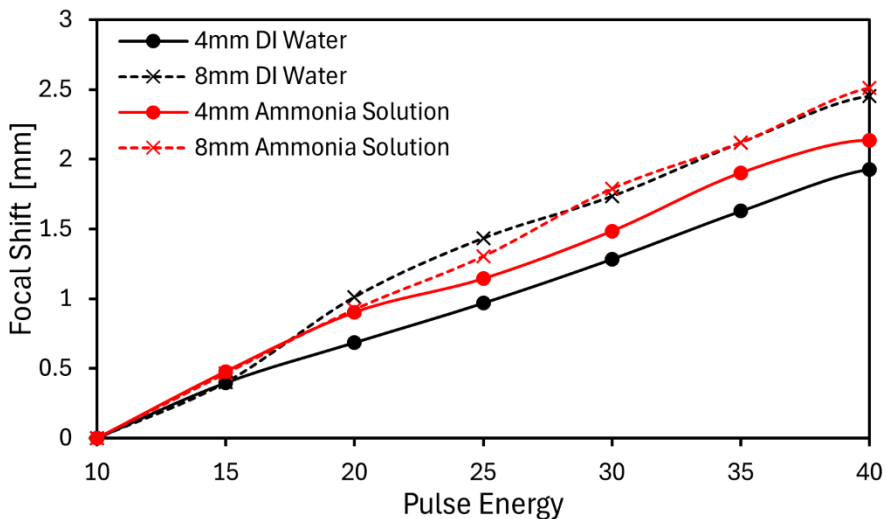


Figure 6.2 Focal shift in relation to applied pulse energy, whereby the pulse energy of 10 μ J was used as the reference point.

Higher pulse energies, although enhancing material removal, also led to non-linear effects such as self-focusing, which shifted the focal point upward, as shown in Figure 6.2, disrupting the laser-crystal interaction. This affected the consistency of the ablation depth, making it challenging to achieve a uniform ablation profile. Furthermore, it was observed that increased distances between the crystal and water surface further enhanced such non-linear effects, resulting in increased focal shift, relative to reduced distances.

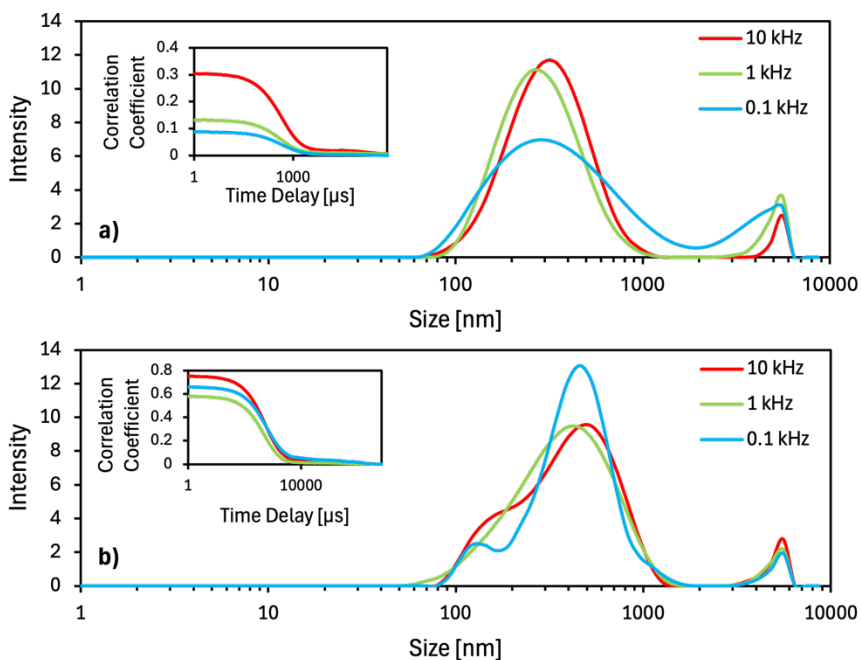


Figure 6.3 DLS size intensity distribution (with inset showing DLS autocorrelation functions) showing the influence of pulse repetition rate on synthesized NP size via fs-PLAL in a) DI water, and b) ammonia solution.

Laser pulse repetition rates were observed to influence the NP size distribution, as discussed in paper III, and further indicated in Figure 6.3. In water, DLS analysis indicated increased productivity with increased repetition rates. In contrast, the overall productivity of PLAL

within ammonia solution remained rather constant within the range of 0.1 – 10 kHz, with lower repetition rates presenting with reduced size distribution. As presented in paper III, higher repetition rates, with an increased number of pulses, led to interactions with the already ablated material in defocused lower-fluence regions, causing laser melting in liquid (LML). This melting led to the coalescence of smaller particles into larger agglomerates, hindering the formation of well-defined NPs. Conversely, lower repetition rates allowed for a more controlled interaction, minimizing LML and helping retain smaller particle sizes.

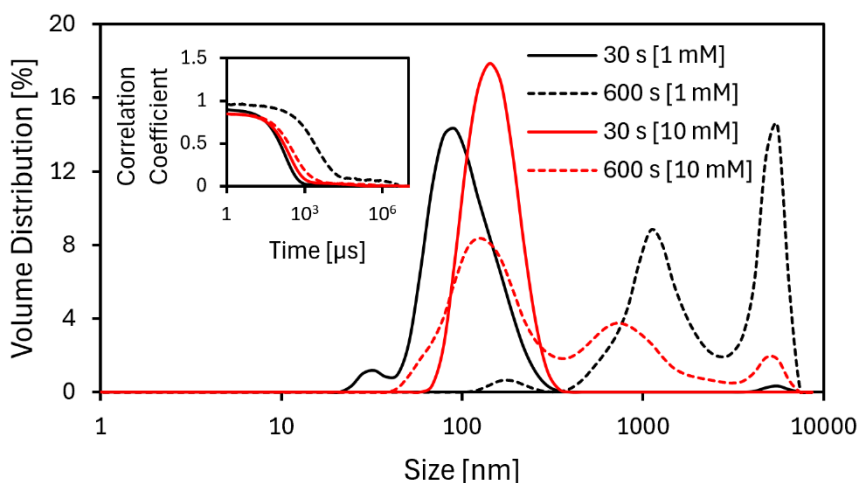


Figure 6.4 DLS volume distribution (with inset showing DLS autocorrelation functions) of nanoparticles synthesized via fs-PLAL in varying concentration of sodium hydroxide solution for 30 s and 600 s respectively.

This is further evident when exploring the influence of ablation time using sodium hydroxide solution, as shown in Figure 6.4. Here, it is clear that increased ablation time, or number of pulses, resulted in a significant shift towards larger size volume distributions regardless of concentration. However, larger concentrations likely assisted in increased colloidal, resulting in a decreased effect of size distribution

increase in proportion with number of laser pulses, as evident by the reduced volume distribution for the secondary and tertiary peaks in the 600 s samples. The influence on solvent, and repetition rate, was further discussed in paper III. Here, it was demonstrated that the reduced ionic strength of DI water resulted in ovoid-like NPs, due to limited colloidal stability, which agglomerated and formed larger structures at higher repetition rates via LML. In contrast, the improved electrostatic repulsion between particles in ammonia solution prevented agglomeration, producing more uniform and spherical NPs at 1 kHz repetition rate. However, an increase in repetition rate to 100 kHz resulted in a large size distribution of agglomerated structures with numerous aspects of LML, shown in Figure 6.5. EDS data is lacking for these structures, therefore there are no conclusions regarding maintenance of stoichiometry for these parameters. Although, the preservation of Yb:YVO₄ NP stoichiometry can be confirmed utilising the parameters discussed in paper III.

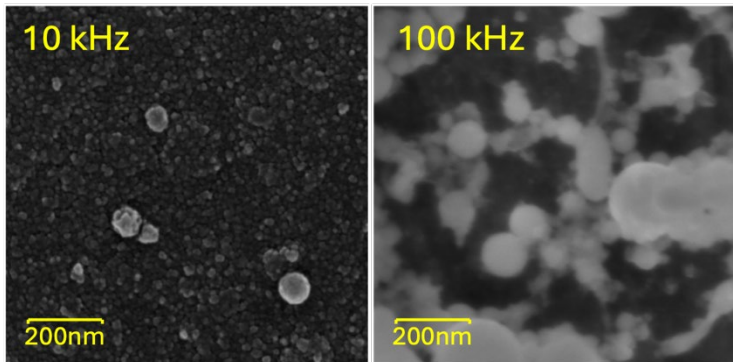


Figure 6.5 SEM imaging of typical Yb:YVO₄ spherical NPs synthesized via fs-PLAL in ammonia solution operating at 10 kHz and 100 kHz, with a view field of 1 μ m.

Here, the interaction between the fs-laser and the material resulted in mechanisms such as Coulomb explosion and multiphoton ionization. These mechanisms led to rapid ionization of the material and efficient

fragmentation of the crystal surface, ultimately allowing for the synthesis of NPs that retained the bulk crystal's stoichiometry (Figure 6.6), which were observed in paper III. This precise energy deposition, unique to fs-lasers, avoided the excessive thermal effects commonly seen in longer-pulsed lasers, such as ns-lasers, which often cause vaporization and loss of stoichiometric integrity.

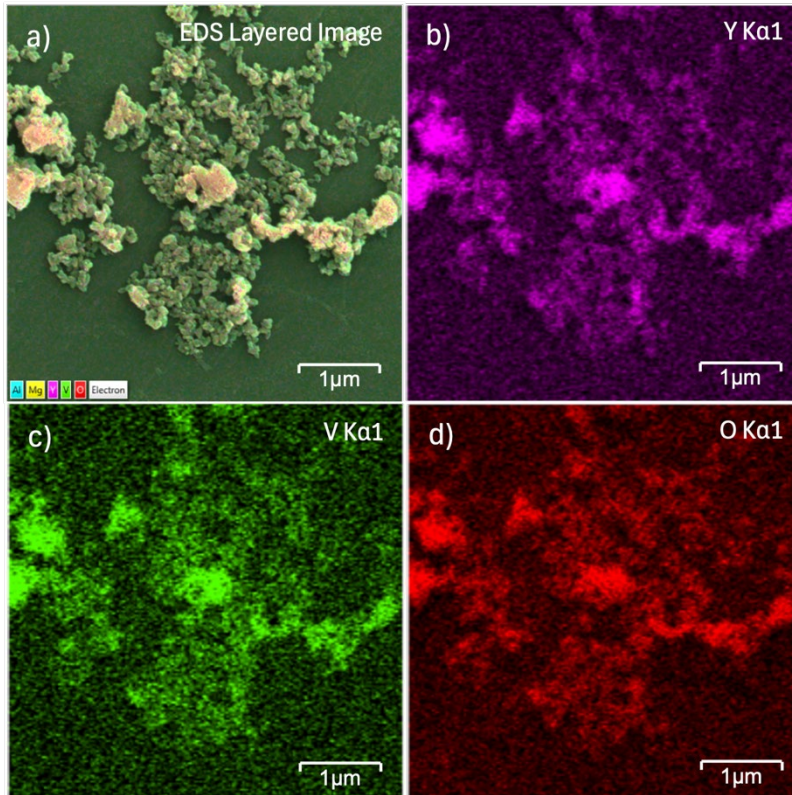


Figure 6.6 EDS of Yb:YVO₄ NP's typically formed via fs-PLAL in DI water.

7 Conclusion and future work

7.1 Conclusion

Investigations into laser-assisted processing yielded critical insights into enhancing material properties across various applications. In polymer-graphene composites, laser parameters like energy density and degree of sintering significantly influence the electrical conductivity and mechanical properties. By optimizing these parameters, the resistance of the composite was minimized, demonstrating laser processing's effectiveness in tailoring conductive pathways and mechanical strength.

Regarding ultrashort pulses used in synthesizing RE-doped NPs, it was found that environmental factors and laser parameters are crucial in determining their final properties. Despite variations in particle shape and size, the stoichiometry of the NPs remained aligned with that of the bulk material. This highlights the precision of ultrashort laser pulses in maintaining desired chemical compositions while engineering specific nanostructures, which are essential for applications requiring strict stoichiometric adherence.

For graphite-based anodes, laser processing significantly enhanced both the structural and electrochemical properties of NG and NGSi composites. Key laser parameters like intensity, scanning speed, interline distance, and processing atmosphere played a crucial role in preventing oxide formation, achieving nanoscale size reduction, increased porosity, and promoting more surface defects and Li-ion intercalation sites. NG anodes showed significant improvements in fast-charging capabilities and specific capacities, while NGSi anodes

demonstrated improved reaction kinetics and structural integrity in cyclic voltammetry testing. However, further characterization regarding battery performance data is lacking, requiring further work.

These findings show the versatility of laser-assisted processing in enhancing the structural, electrical, and mechanical properties of diverse materials, paving the way for high-performance applications across various industries.

7.2 Social and ethical considerations

The use of lasers in material processing has both environmental and ethical implications. On the positive side, lasers offer precision and efficiency, potentially reducing material waste and energy consumption compared to traditional methods. This efficiency minimizes excessive material removal and enables targeted energy use, lowering overall resource consumption. However, the high energy demands for laser operations and the production of laser systems can contribute to greenhouse gas emissions, and by-products such as fumes and particulate matter which may pose health and environmental risks if not managed properly. Consequently, advancements in laser technology should focus on enhancing energy efficiency and incorporating sustainable materials, alongside proper recycling protocols to minimize environmental impact.

Ethical considerations also arise with the advancement of laser technology. Increased automation raises concerns about job displacement, necessitating strategies for worker retraining. Additionally, the energy consumption and waste generated by high-powered lasers must be managed responsibly to avoid exacerbating environmental degradation. Access to advanced laser technologies may be uneven, potentially widening inequalities between well-

funded organizations and those with limited resources. Finally, the potential misuse of lasers in harmful applications, such as weaponry, highlights the need for responsible development focused on societal benefits.

The societal impact of advancing laser technology in material processing is significant. The precision of lasers can revolutionize manufacturing, leading to high-quality, complex components and lower production costs, ultimately improving quality of life. In healthcare, lasers enhance diagnostics and therapies, resulting in less invasive treatment options and improved patient outcomes. However, while automation may displace some manual labour positions, it also creates opportunities for skilled roles in technology development and maintenance, necessitating adaptive education and training programs. Balancing these advances with consideration for workforce impact, economic equity, and access to technology is crucial to ensure that the benefits of laser material processing are widely shared.

7.3 Future work

There are several promising avenues for further research based on the findings in this thesis. A primary area for expansion involves laser parameter optimization of electrically conductive polymer-graphene composites, specifically within SLS applications. Due to limitations in experimental scope, laser processing has been conducted without access to an industrial SLS machine, using a single 1064nm CW laser-source, with alternative techniques such as coatings and direct laser processing on heated powder samples. Future experiments using an industrial SLS machine would enable precise control over critical environmental factors, such as ambient temperature stability, roller pressure consistency, and uniform powder layer depth, providing a

foundation for parameter optimization. Furthermore, the use of alternate laser sources, such as a CO₂ laser, would further enhance the level of optimization to be applied across various laser system for SLS applications. In addition to enabling standard sample production (e.g., ISO dog-bone specimens) for enhanced mechanical characterization, such as Young's modulus testing. Furthermore, additional work could explore alternative NP composites, such as carbon nanotubes or metal oxides, to assess their impact on conductivity and mechanical properties under SLS conditions with optimized laser parameters. Additionally, expanding into wear resistance and fatigue testing could provide insights into the long-term stability of these composites, particularly for applications in electronics, aerospace, or medical devices, where durability and conductive properties are critical.

Future research on the laser processing of graphite-based anodes offers substantial potential. Initially, it's evident that laser processing performed within this study presented with a limited depth effect, whereby optimizations are required to process the entire electrode depth. Additional wavelengths should be studied in relation to absorption depth and processing depth, tied to varied coating thickness and possibly incorporating multiple layers post-processing to maximize porous material structure. Moreover, utilizing periodic hole/line structures via fs-laser ablation in addition to current laser processing techniques may prove advantageous in improving rate capability during galvanostatic charge-discharge cycling. In the study on NGSi composite anodes, performance comparisons were limited to cyclic voltammetry testing. Future work should incorporate galvanostatic charge-discharge testing to fully assess capacity, coulombic efficiency, and cycling stability across a broad range of charge/discharge rates. Additionally, post-mortem studies could also

reveal insights relating into lithium plating or dendrite formation, providing a clearer picture of failure mechanisms and structural degradation following post-cycling. This would enable a more direct comparison between laser-processed NGSi and non-processed samples, offering clearer insights into the practical energy storage benefits. Expanding on material compositions could also be beneficial. For example, exploring the effect of adding conductive binders or other nanostructured carbon materials may further enhance conductivity and stability under cycling conditions. Examining the effect of these modifications on both performance and thermal stability in different environmental conditions could be especially relevant for high-power applications such as EVs and grid storage.

Future research on RE-doped NP synthesis through PLAL presents numerous opportunities for advancing production efficiency and NP quality. Exploring different RE-doped crystals, such as Er or Nd-doped could expand optical applications via an exploration of how composition affects NP morphology and optical properties. Using additional laser wavelengths in PLAL could offer valuable insights into wavelength-specific effects on NP size, shape, and productivity, helping identify the optimal conditions for targeted NP characteristics. Additionally, examining multi-beam laser setups may further enhance ablation productivity. Implementing a flow-cell setup with polygon scanners would enable high repetition rates without pulse overlap and LML effects, facilitating large-scale production. The inclusion of varied solvents and surfactants could further enhance colloidal stability, minimizing aggregation and improving NP distribution. Embedding synthesized NPs in hybrid RE-doped silica fibers could combine unique optical properties with silica's mechanical stability, advancing applications in fiber lasers and other photonic devices.

While the presented works showcase the technical potential of laser processing for NP synthesis and material optimization, the economic feasibility of this approach remains unexplored. Assessing the cost efficiency of laser processing, particularly in comparison to conventional production methods, is essential for industrial applications. Key factors to consider include energy consumption, equipment costs, and scalability relative to production rates. Understanding these economic dimensions will be crucial for positioning laser processing as a competitive alternative in large-scale manufacturing.

7.4 Author's contributions

The information regarding the contributions of each author is presented in Table 7.1

Table 7.1 Author's contributions, whereby the acronyms and their associated authors are as follows respectively: L.B - Luke Bond, H.A - Henrik Andersson, M.E - Magnus Engholm, J.Ö - Jonas Örtengren, M.L - Magnus Larsson, E.J - Ellinor Jönsson.

Contribution	Paper I	Paper II	Paper III	Paper IV
Conceptualization of the idea	L.B, H.A, and M.E	L.B, H.A, and M.E	L.B, and M.E	L.B, H.A, M.H, and M.E
Experimental work	L.B	L.B	L.B, and E.J	L.B
Collecting the data	L.B	L.B	L.B, and E.J	L.B
Elaboration of the data	L.B	L.B	L.B, and E.J	L.B, and M.E
Writing the first draft	L.B	L.B	L.B	L.B
Editing the manuscript	L.B, H.A, and M.E	L.B, H.A, and M.E	L.B, and M.E	L.B, and M.E
Revising the manuscript	L.B, H.A, M.E, J.Ö, and M.L	L.B, H.A, and M.E	L.B, E.J, H.A, and M.E	L.B, H.A, M.E, and M.H

Bibliography

- ¹ Z. Wang, B. Zhang, J. Liu, Y. Song, and H. Zhang, "Recent developments in mid-infrared fiber lasers: Status and challenges," *Optics & Laser Technology* **132**, 106497 (2020).
- ² R. Li, B. Lin, Y. Liu, M. Dong, and S. Zhao, "A Survey on Laser Space Network: Terminals, Links, and Architectures," *IEEE Access* **10**, 34815–34834 (2022).
- ³ M. Lancry, and B. Poumellec, "UV laser processing and multiphoton absorption processes in optical telecommunication fiber materials," *Physics Reports* **523**(4), 207–229 (2013).
- ⁴ T. Thaweeskulchai, K. Sakdaphetsiri, and A. Schulte, "Ten years of laser-induced graphene: impact and future prospect on biomedical, healthcare, and wearable technology," *Microchim Acta* **191**(5), 292 (2024).
- ⁵ E. Sharon, I. Snast, M. Lapidot, R. Kaftory, D. Mimouni, E. Hodak, and A. Levi, "Laser Treatment for Non-Melanoma Skin Cancer: A Systematic Review and Meta-Analysis," *Am J Clin Dermatol* **22**(1), 25–38 (2021).
- ⁶ P. Jamshidi, M. Aristizabal, W. Kong, V. Villapun, S.C. Cox, L.M. Grover, and M.M. Attallah, "Selective Laser Melting of Ti-6Al-4V: The Impact of Post-processing on the Tensile, Fatigue and Biological Properties for Medical Implant Applications," *Materials* **13**(12), 2813 (2020).
- ⁷ E. Schena, P. Saccomandi, and Y. Fong, "Laser Ablation for Cancer: Past, Present and Future," *Journal of Functional Biomaterials* **8**(2), 19 (2017).
- ⁸ H. Breuer, N. Krasner, T. Okunata, and D. Sliney, *Applied Laser Medicine* (Springer Science & Business Media, 2012).
- ⁹ Y.C. Shin, B. Wu, S. Lei, G.J. Cheng, and Y. Lawrence Yao, "Overview of Laser Applications in Manufacturing and Materials Processing in Recent Years," *J. Manuf. Sci. Eng.-Trans. ASME* **142**(11), 110818 (2020).
- ¹⁰ L. Thijs, K. Kempen, J.-P. Kruth, and J. Van Humbeeck, "Fine-structured aluminium products with controllable texture by selective laser melting of pre-alloyed AlSi10Mg powder," *Acta Materialia* **61**(5), 1809–1819 (2013).

- ¹¹ S. Lei, X. Zhao, X. Yu, A. Hu, S. Vukelic, M.B.G. Jun, H.-E. Joe, Y.L. Yao, and Y.C. Shin, "Ultrafast Laser Applications in Manufacturing Processes: A State-of-the-Art Review," *Journal of Manufacturing Science and Engineering* **142**(031005), (2020).
- ¹² L. Orazi, L. Romoli, M. Schmidt, and L. Li, "Ultrafast laser manufacturing: from physics to industrial applications," *CIRP Annals* **70**(2), 543–566 (2021).
- ¹³ D. Zhang, and H. Wada, "Laser Ablation in Liquids for Nanomaterial Synthesis and Applications," in *Handbook of Laser Micro- and Nano-Engineering*, edited by K. Sugioka, (Springer International Publishing, Cham, 2020), pp. 1–35.
- ¹⁴ D. Zhang, B. Gökce, and S. Barcikowski, "Laser Synthesis and Processing of Colloids: Fundamentals and Applications," *Chem. Rev.* **117**(5), 3990–4103 (2017).
- ¹⁵ T.-S.D. Le, H.-P. Phan, S. Kwon, S. Park, Y. Jung, J. Min, B.J. Chun, H. Yoon, S.H. Ko, S.-W. Kim, and Y.-J. Kim, "Recent Advances in Laser-Induced Graphene: Mechanism, Fabrication, Properties, and Applications in Flexible Electronics," *Advanced Functional Materials* **32**(48), 2205158 (2022).
- ¹⁶ J. Ion, *Laser Processing of Engineering Materials: Principles, Procedure and Industrial Application* (Elsevier, 2005).
- ¹⁷ J. Dutta Majumdar, and I. Manna, "Laser material processing," *International Materials Reviews* **56**(5–6), 341–388 (2011).
- ¹⁸ W. Han, L. Kong, and M. Xu, "Advances in selective laser sintering of polymers," *Int. J. Extrem. Manuf.* **4**(4), 042002 (2022).
- ¹⁹ J. Krieglner, M. Binzer, and M.F. Zaeh, "Process strategies for laser cutting of electrodes in lithium-ion battery production," *Journal of Laser Applications* **33**(1), 012006 (2020).
- ²⁰ Naresh, and P. Khatak, "Laser cutting technique: A literature review," *Materials Today: Proceedings* **56**, 2484–2489 (2022).
- ²¹ W. Pfleging, "Recent progress in laser texturing of battery materials: a review of tuning electrochemical performances, related material development, and prospects for large-scale manufacturing," *Int. J. Extrem. Manuf.* **3**(1), 012002 (2020).
- ²² S. Katayama, *Fundamentals and Details of Laser Welding* (Springer, Singapore, 2020).

- ²³ N. Khosla, J. Narayan, R. Narayan, X.-G. Sun, and M.P. Paranthaman, "Microstructure and defect engineering of graphite anodes by pulsed laser annealing for enhanced performance of lithium-ion batteries," *Carbon* **205**, 214–225 (2023).
- ²⁴ M. Liu, J. Wu, and H. Cheng, "Effects of laser processing parameters on properties of laser-induced graphene by irradiating CO₂ laser on polyimide," *Sci. China Technol. Sci.* **65**(1), 41–52 (2022).
- ²⁵ B.F. Mohazzab, B. Jaleh, A. Fattah-alhosseini, F. Mahmoudi, and A. Momeni, "Laser surface treatment of pure titanium: Microstructural analysis, wear properties, and corrosion behavior of titanium carbide coatings in Hank's physiological solution," *Surfaces and Interfaces* **20**, 100597 (2020).
- ²⁶ I. Y. Khairani, G. Mínguez-Vega, C. Doñate-Buendía, and B. Gökce, "Green nanoparticle synthesis at scale: a perspective on overcoming the limits of pulsed laser ablation in liquids for high-throughput production," *Physical Chemistry Chemical Physics* **25**(29), 19380–19408 (2023).
- ²⁷ H. Du, V. Castaing, D. Guo, and B. Viana, "Rare-earths doped-nanoparticles prepared by pulsed laser ablation in liquids," *Ceramics International* **46**(16, Part B), 26299–26308 (2020).
- ²⁸ A.V. Kabashin, A. Singh, M.T. Swihart, I.N. Zavestovskaya, and P.N. Prasad, "Laser-Processed Nanosilicon: A Multifunctional Nanomaterial for Energy and Healthcare," *ACS Nano* **13**(9), 9841–9867 (2019).
- ²⁹ M. Schmid, A. Amado, and K. Wegener, "Polymer powders for selective laser sintering (SLS)," *AIP Conference Proceedings* **1664**(1), 160009 (2015).
- ³⁰ R. Streubel, S. Barcikowski, and B. Gökce, "Continuous multigram nanoparticle synthesis by high-power, high-repetition-rate ultrafast laser ablation in liquids," *Opt. Lett.*, OL **41**(7), 1486–1489 (2016).
- ³¹ P. Sehrawat, A. Shabir, Abid, C.M. Julien, and S.S. Islam, "Recent trends in silicon/graphene nanocomposite anodes for lithium-ion batteries," *Journal of Power Sources* **501**, 229709 (2021).
- ³² L. Sun, Y. Liu, R. Shao, J. Wu, R. Jiang, and Z. Jin, "Recent progress and future perspective on practical silicon anode-based lithium ion batteries," *Energy Storage Materials* **46**, 482–502 (2022).

- ³³ B. Liu, P. Wu, Y. Li, H. Zhu, and L. Lv, "Design and Photoelectric Performance of Perfect Solar Absorber Based on GaAs Grating," *Frontiers in Materials* **8**, (2022).
- ³⁴ M.V. Shugaev, M. He, Y. Levy, A. Mazzi, A. Miotello, N.M. Bulgakova, and L.V. Zhigilei, "Laser-Induced Thermal Processes: Heat Transfer, Generation of Stresses, Melting and Solidification, Vaporization, and Phase Explosion," in *Handbook of Laser Micro- and Nano-Engineering*, edited by K. Sugioka, (Springer International Publishing, Cham, 2021), pp. 83–163.
- ³⁵ D. Bäuerle, *Laser Processing and Chemistry* (Springer Science & Business Media, 2013).
- ³⁶ K. Ujihara, "Reflectivity of metals at high temperatures," *IEEE Journal of Quantum Electronics* **8**(6), 567–568 (1972).
- ³⁷ A. Sharma, M.N. Slipchenko, M.N. Shneider, X. Wang, K.A. Rahman, and A. Shashurin, "Counting the electrons in a multiphoton ionization by elastic scattering of microwaves," *Sci Rep* **8**(1), 2874 (2018).
- ³⁸ S.S. Harilal, J.R. Freeman, P.K. Diwakar, and A. Hassanein, "Femtosecond Laser Ablation: Fundamentals and Applications," in *Laser-Induced Breakdown Spectroscopy: Theory and Applications*, edited by S. Musazzi and U. Perini, (Springer, Berlin, Heidelberg, 2014), pp. 143–166.
- ³⁹ G. Padmanabham, and R. Bathe, "Laser Materials Processing for Industrial Applications," *Proc. Natl. Acad. Sci., India, Sect. A Phys. Sci.* **88**(3), 359–374 (2018).
- ⁴⁰ J.R. Lawrence, *Advances in Laser Materials Processing: Technology, Research and Applications* (Woodhead Publishing, 2017).
- ⁴¹ F. Lupone, E. Padovano, F. Casamento, and C. Badini, "Process Phenomena and Material Properties in Selective Laser Sintering of Polymers: A Review," *Materials* **15**(1), 183 (2022).
- ⁴² N. Chen, J. Zhao, J. Wei, H. Xiao, L. Li, J. Liu, N. Yu, and N. He, "Influence of laser-processed surfaces on heat transfer performance of microflow channels," *Case Studies in Thermal Engineering* **52**, 103624 (2023).
- ⁴³ H. Zhou, J. Lee, M. Kang, H. Kim, H. Lee, and J.B. In, "All laser-based fabrication of microchannel heat sink," *Materials & Design* **221**, 110968 (2022).

- ⁴⁴ K.-H. Chen, M.J. Namkoong, V. Goel, C. Yang, S. Kazemiabnavi, S.M. Mortuza, E. Kazyak, J. Mazumder, K. Thornton, J. Sakamoto, and N.P. Dasgupta, "Efficient fast-charging of lithium-ion batteries enabled by laser-patterned three-dimensional graphite anode architectures," *Journal of Power Sources* **471**, 228475 (2020).
- ⁴⁵ L. Hille, L. Xu, J. Keilhofer, S. Stock, J. Kriegler, and M.F. Zaeh, "Laser structuring of graphite anodes and NMC cathodes – Proportionate influence on electrode characteristics and cell performance," *Electrochimica Acta* **392**, 139002 (2021).
- ⁴⁶ Q. Meng, X. Song, S. Han, F. Abbassi, Z. Zhou, B. Wu, X. Wang, and S. Araby, "Mechanical and functional properties of polyamide/graphene nanocomposite prepared by chemicals free-approach and selective laser sintering," *Composites Communications* **36**, 101396 (2022).
- ⁴⁷ D. Zhang, Z. Li, and K. Sugioka, "Laser ablation in liquids for nanomaterial synthesis: diversities of targets and liquids," *J. Phys. Photonics* **3**(4), 042002 (2021).
- ⁴⁸ B. Chen, R. Davies, Y. Liu, N. Yi, D. Qiang, Y. Zhu, and O. Ghita, "Laser sintering of graphene nanoplatelets encapsulated polyamide powders," *Additive Manufacturing* **35**, 101363 (2020).
- ⁴⁹ R. Navik, H. Tan, H. Zhang, Z. Liu, Q. Xiang, L. Shi, S. Lu, and Y. Zhao, "Scalable production of polyamide-6/graphene composites with enhanced electromagnetic shielding and thermal conductivity," *Chemical Engineering Journal* **471**, 144445 (2023).
- ⁵⁰ G. Rollo, A. Ronca, P. Cerruti, X.P. Gan, G. Fei, H. Xia, G. Gorokhov, D. Bychanok, P. Kuzhir, M. Lavorgna, and L. Ambrosio, "On the Synergistic Effect of Multi-Walled Carbon Nanotubes and Graphene Nanoplatelets to Enhance the Functional Properties of SLS 3D-Printed Elastomeric Structures," *Polymers* **12**(8), 1841 (2020).
- ⁵¹ D.Z. Chen, S. Lao, J.H. Koo, M. Londa, and Z. Alabdullatif, "Powder Processing and Properties Characterization of Polyamide 11-Graphene Nanocomposites for Selective Laser Sintering," (2010).
- ⁵² H. Zhang, Y. Yang, D. Ren, L. Wang, and X. He, "Graphite as anode materials: Fundamental mechanism, recent progress and advances," *Energy Storage Materials* **36**, 147–170 (2021).

- ⁵³ L.S. Roselin, R.-S. Juang, C.-T. Hsieh, S. Sagadevan, A. Umar, R. Selvin, and H.H. Hegazy, "Recent Advances and Perspectives of Carbon-Based Nanostructures as Anode Materials for Li-ion Batteries," *Materials* **12**(8), 1229 (2019).
- ⁵⁴ J. Kim, S.M. Nithya Jeghan, and G. Lee, "Superior fast-charging capability of graphite anode via facile surface treatment for lithium-ion batteries," *Microporous and Mesoporous Materials* **305**, 110325 (2020).
- ⁵⁵ Y. Lee, S.M.N. Jeghan, and G. Lee, "Boost charging lithium-ion battery using expanded graphite anode with enhanced performance," *Materials Letters* **299**, 130077 (2021).
- ⁵⁶ Z. Yan, S. Yi, X. Li, J. Jiang, D. Yang, and N. Du, "A scalable silicon/graphite anode with high silicon content for high-energy lithium-ion batteries," *Materials Today Energy* **31**, 101225 (2023).
- ⁵⁷ K. Feng, M. Li, W. Liu, A.G. Kashkooli, X. Xiao, M. Cai, and Z. Chen, "Silicon-Based Anodes for Lithium-Ion Batteries: From Fundamentals to Practical Applications," *Small* **14**(8), 1702737 (2018).
- ⁵⁸ M. Qian, Y.S. Zhou, Y. Gao, J.B. Park, T. Feng, S.M. Huang, Z. Sun, L. Jiang, and Y.F. Lu, "Formation of graphene sheets through laser exfoliation of highly ordered pyrolytic graphite," *Applied Physics Letters* **98**(17), 173108 (2011).
- ⁵⁹ E. Alhajji, F. Zhang, and H.N. Alshareef, "Status and Prospects of Laser-Induced Graphene for Battery Applications," *Energy Technology* **9**(10), 2100454 (2021).
- ⁶⁰ J. Kriegler, L. Hille, S. Stock, L. Kraft, J. Hagemeister, J.B. Habedank, A. Jossen, and M.F. Zaeh, "Enhanced performance and lifetime of lithium-ion batteries by laser structuring of graphite anodes," *Applied Energy* **303**, 117693 (2021).
- ⁶¹ H. Wang, O. Odawara, and H. Wada, "One-step preparation of YVO₄:Eu³⁺ nanoparticles by pulsed laser ablation," *Journal of Alloys and Compounds* **683**, 1–6 (2016).
- ⁶² H. Wang, O. Odawara, and H. Wada, "Morphology and optical properties of YVO₄:Eu³⁺ nanoparticles fabricated by laser ablation in ethanol," *Applied Surface Science* **425**, 689–695 (2017).
- ⁶³ Z. Lu, N. Vakula, M. Ude, M. Cabié, T. Neisius, F. Orange, F. Pigeonneau, L. Petit, and W. Blanc, "YbPO₄ crystals in as-drawn silica-based optical fibers," *Optical Materials* **138**, 113644 (2023).

- ⁶⁴ D.M. Panaitescu, R.A. Gabor, A.N. Frone, and E. Vasile, "Influence of Thermal Treatment on Mechanical and Morphological Characteristics of Polyamide 11/Cellulose Nanofiber Nanocomposites," *Journal of Nanomaterials* **2015**(1), 136204 (2015).
- ⁶⁵ E.B. Mubofu, "Castor oil as a potential renewable resource for the production of functional materials," *Sustain Chem Process* **4**(1), 11 (2016).
- ⁶⁶ G.R. Esposito, T.J. Dingemans, and R.A. Pearson, "Changes in polyamide 11 microstructure and chemistry during selective laser sintering," *Additive Manufacturing* **48**, 102445 (2021).
- ⁶⁷ W.S. Tey, C. Cai, and K. Zhou, "A Comprehensive Investigation on 3D Printing of Polyamide 11 and Thermoplastic Polyurethane via Multi Jet Fusion," *Polymers* **13**(13), 2139 (2021).
- ⁶⁸ L. Martino, L. Basilissi, H. Farina, M.A. Ortenzi, E. Zini, G. Di Silvestro, and M. Scandola, "Bio-based polyamide 11: Synthesis, rheology and solid-state properties of star structures," *European Polymer Journal* **59**, 69–77 (2014).
- ⁶⁹ M.A. Dechet, A. Goblirsch, S. Romeis, M. Zhao, F.J. Lanyi, J. Kaschta, D.W. Schubert, D. Drummer, W. Peukert, and J. Schmidt, "Production of polyamide 11 microparticles for Additive Manufacturing by liquid-liquid phase separation and precipitation," *Chemical Engineering Science* **197**, 11–25 (2019).
- ⁷⁰ I. Fidan, O. Huseynov, M.A. Ali, S. Alkunte, M. Rajeshirke, A. Gupta, S. Hasanov, K. Tantawi, E. Yasa, O. Yilmaz, J. Loy, V. Popov, and A. Sharma, "Recent Inventions in Additive Manufacturing: Holistic Review," *Inventions* **8**(4), 103 (2023).
- ⁷¹ H. Wu, W.P. Fahy, S. Kim, H. Kim, N. Zhao, L. Pilato, A. Kafi, S. Bateman, and J.H. Koo, "Recent developments in polymers/polymer nanocomposites for additive manufacturing," *Progress in Materials Science* **111**, 100638 (2020).
- ⁷² S.R. Athreya, K. Kalaitzidou, and S. Das, "Processing and characterization of a carbon black-filled electrically conductive Nylon-12 nanocomposite produced by selective laser sintering," *Materials Science and Engineering: A* **527**(10), 2637–2642 (2010).
- ⁷³ C.A. Chatham, T.E. Long, and C.B. Williams, "A review of the process physics and material screening methods for polymer powder

bed fusion additive manufacturing," *Progress in Polymer Science* **93**, 68–95 (2019).

⁷⁴ R. Brighenti, M.P. Cosma, L. Marsavina, A. Spagnoli, and M. Terzano, "Laser-based additively manufactured polymers: a review on processes and mechanical models," *J Mater Sci* **56**(2), 961–998 (2021).

⁷⁵ X. Wei, D. Li, W. Jiang, Z. Gu, X. Wang, Z. Zhang, and Z. Sun, "3D Printable Graphene Composite," *Sci Rep* **5**(1), 11181 (2015).

⁷⁶ H. Shen, W. Wu, H. Hu, Z. Rui, J. Ye, and C. Zhang, "Preparation of carbon black/graphene nanosheets/PP composites with 3D separated conductive networks based on selective laser sintering," *Polymer Composites* **44**(6), 3522–3534 (2023).

⁷⁷ F.G. Torres, O.P. Troncoso, L. Rodriguez, and G.E. De-la-Torre, "Sustainable synthesis, reduction and applications of graphene obtained from renewable resources," *Sustainable Materials and Technologies* **29**, e00310 (2021).

⁷⁸ B. Chen, S. Berretta, K. Evans, K. Smith, and O. Ghita, "A primary study into graphene/polyether ether ketone (PEEK) nanocomposite for laser sintering," *Applied Surface Science* **428**, 1018–1028 (2018).

⁷⁹ D.H. Seo, S. Pineda, J. Fang, Y. Gozukara, S. Yick, A. Bendavid, S.K.H. Lam, A.T. Murdock, A.B. Murphy, Z.J. Han, and K. (Ken) Ostrikov, "Single-step ambient-air synthesis of graphene from renewable precursors as electrochemical genosensor," *Nat Commun* **8**(1), 14217 (2017).

⁸⁰ T. Smausz, B. Kondász, T. Gera, T. Ajtai, N. Utry, M. Pintér, G. Kiss-Albert, J. Budai, Z. Bozóki, G. Szabo, and B. Hopp, "Determination of UV–visible–NIR absorption coefficient of graphite bulk using direct and indirect methods," *Applied Physics A* **123**, (2017).

⁸¹ M. Torkunov, K. Shiyanova, E. Verkhova, V. Yulovskaya, N. Ryvkina, V. Melnikov, M. Gudkov, and I. Chmutin, "Powders of rGO-coated polyamide with special electrical properties for SLS 3D printing," *Journal of Composite Materials* **57**(14), 2233–2242 (2023).

⁸² C.A. Biffi, J. Fiocchi, P. Bassani, and A. Tuissi, "Continuous wave vs pulsed wave laser emission in selective laser melting of AlSi10Mg parts with industrial optimized process parameters: Microstructure and mechanical behaviour," *Additive Manufacturing* **24**, 639–646 (2018).

- ⁸³ X. Huang, C. Zhi, Y. Lin, H. Bao, G. Wu, P. Jiang, and Y.-W. Mai, "Thermal conductivity of graphene-based polymer nanocomposites," *Materials Science and Engineering: R: Reports* **142**, 100577 (2020).
- ⁸⁴ R. Patil, M. Phadatore, N. Blomquist, J. Örtengren, M. Hummelgård, J. Meshram, D. Dubal, and H. Olin, "Highly Stable Cycling of Silicon-Nanographite Aerogel-Based Anode for Lithium-Ion Batteries," *ACS Omega* **6**(10), 6600–6606 (2021).
- ⁸⁵ M. Phadatore, R. Patil, N. Blomquist, S. Forsberg, J. Örtengren, M. Hummelgård, J. Meshram, G. Hernández, D. Brandell, K. Leifer, S.K.M. Sathyanath, and H. Olin, "Silicon-Nanographite Aerogel-Based Anodes for High Performance Lithium Ion Batteries," *Sci Rep* **9**(1), 14621 (2019).
- ⁸⁶ X. Cai, L. Lai, Z. Shen, and J. Lin, "Graphene and graphene-based composites as Li-ion battery electrode materials and their application in full cells," *J. Mater. Chem. A* **5**(30), 15423–15446 (2017).
- ⁸⁷ R. Raccichini, A. Varzi, D. Wei, and S. Passerini, "Critical Insight into the Relentless Progression Toward Graphene and Graphene-Containing Materials for Lithium-Ion Battery Anodes," *Advanced Materials* **29**(11), 1603421 (2017).
- ⁸⁸ Y.P. Wu, E. Rahm, and R. Holze, "Carbon anode materials for lithium ion batteries," *Journal of Power Sources* **114**(2), 228–236 (2003).
- ⁸⁹ E. Yoo, J. Kim, E. Hosono, H. Zhou, T. Kudo, and I. Honma, "Large Reversible Li Storage of Graphene Nanosheet Families for Use in Rechargeable Lithium Ion Batteries," *Nano Lett.* **8**(8), 2277–2282 (2008).
- ⁹⁰ H. Xiang, K. Zhang, G. Ji, J.Y. Lee, C. Zou, X. Chen, and J. Wu, "Graphene/nanosized silicon composites for lithium battery anodes with improved cycling stability," *Carbon* **49**(5), 1787–1796 (2011).
- ⁹¹ N. Palina, T. Mueller, S. Mohanti, and A. ABERLE, "Laser assisted boron doping of silicon wafer solar cells using nanosecond and picosecond laser pulses," *Conference Record of the IEEE Photovoltaic Specialists Conference*, 002193–002197 (2011).
- ⁹² V. Amendola, and M. Meneghetti, "What controls the composition and the structure of nanomaterials generated by laser ablation in liquid solution?," *Phys. Chem. Chem. Phys.* **15**(9), 3027–3046 (2013).
- ⁹³ S. Dittrich, S. Kohsakowski, B. Wittek, C. Hengst, B. Gökce, S. Barcikowski, and S. Reichenberger, "Increasing the Size-Selectivity in

Laser-Based g/h Liquid Flow Synthesis of Pt and PtPd Nanoparticles for CO and NO Oxidation in Industrial Automotive Exhaust Gas Treatment Benchmarking," *Nanomaterials* **10**(8), 1582 (2020).

⁹⁴ M.H. Mahdiah, and B. Fattahi, "Size properties of colloidal nanoparticles produced by nanosecond pulsed laser ablation and studying the effects of liquid medium and laser fluence," *Applied Surface Science* **329**, 47–57 (2015).

⁹⁵ M. Kim, S. Osone, T. Kim, H. Higashi, and T. Seto, "Synthesis of Nanoparticles by Laser Ablation: A Review," *KONA* **34**, 80–90 (2017).

⁹⁶ K. Mehta, S. Soumyashree, J. Pandya, P. Singh, R.K. Kushawaha, P. Kumar, S. Shinde, J. Saha, and P.K. Baruah, "Impact of viscosity of liquid on nanoparticles synthesized by laser ablation in liquid: An experimental and theoretical investigation," *Appl. Phys. A* **129**(5), 388 (2023).

⁹⁷ T. Tsuji, D.-H. Thang, Y. Okazaki, M. Nakanishi, Y. Tsuboi, and M. Tsuji, "Preparation of silver nanoparticles by laser ablation in polyvinylpyrrolidone solutions," *Applied Surface Science* **254**(16), 5224–5230 (2008).

⁹⁸ H. Zeng, X.-W. Du, S.C. Singh, S.A. Kulinich, S. Yang, J. He, and W. Cai, "Nanomaterials via Laser Ablation/Irradiation in Liquid: A Review," *Advanced Functional Materials* **22**(7), 1333–1353 (2012).

⁹⁹ M.-R. Kalus, S. Barcikowski, and B. Gökce, "How the Physicochemical Properties of the Bulk Material Affect the Ablation Crater Profile, Mass Balance, and Bubble Dynamics During Single-Pulse, Nanosecond Laser Ablation in Water," *Chemistry – A European Journal* **27**(19), 5978–5991 (2021).

¹⁰⁰ M. Soharab, I. Bhaumik, R. Bhatt, A. Saxena, A.K. Karnal, S. Satapathy, and P.K. Gupta, "Effect of Yb doping on the crystal structure, polarization dependent optical absorption and photoluminescence of Yb:YVO₄ single crystal grown by optical floating zone technique," *Journal of Alloys and Compounds* **649**, 766–771 (2015).

¹⁰¹ H. Zhang, X. Meng, L. Zhu, P. Wang, X. Liu, Z. Yang, J. Dawes, and P. Dekker, "Growth, Morphology and Characterization of Yb : YVO₄ Crystal," *Physica Status Solidi (a)* **175**(2), 705–710 (1999).

¹⁰² C. Kränkel, D. Fagundes-Peters, S.T. Fredrich, J. Johannsen, M. Mond, G. Huber, M. Bernhagen, and R. Uecker, "Continuous wave laser operation of Yb³⁺:YVO₄," *Appl Phys B* **79**(5), 543–546 (2004).